

# POLITECNICO DI TORINO

Master degree in Biomedical Engineering



**Development of experimental protocol to validate  
and verify a patient specific TKA FE model during a  
passive TKA movement**

**Italian supervisors:**

**Prof.ssa Cristina Bignardi**

**Prof. Alberto Audenino**

**Belgian supervisor:**

**Prof. Bernardo Innocenti**

**Candidato:**

**Anna Aimar**

*Alla mia famiglia.*

# Table of contents

<b>Abstract</b> .....	3
<b>Sommario</b> .....	4
<b>1. Anatomy and biomechanics of the knee joint</b> .....	5
1.1. Anatomy of the knee joint.....	5
1.2. Biomechanics of the knee joint.....	8
1.2.1. Kinematics of the knee joint.....	8
1.2.2. Kinetics of the knee joint.....	9
<b>2. Total knee arthroplasty</b> .....	10
2.1. Introduction.....	10
2.2. TKA components.....	11
2.3. TKA standard design implant.....	12
<b>3. Aim of the activity</b> .....	13
3.1. Introduction to the analysis.....	13
3.2. State of art and background.....	13
3.3. Workflow and Research questions.....	13
<b>4. Experimental model</b> .....	16
4.1. Pilot tests and protocol difficulties.....	16
4.2. Final test: definition of a complete experimental protocol for passive movement of implanted knee.....	17
4.2.1. Methodological sequence.....	17
4.2.1.1. Preparation of the test.....	17
4.2.1.2. Passive test and kinematic real time measurement.....	27
<b>5. Mechanical characterization of the MCL and LCL</b> .....	31
5.1 . Tensile test.....	31
5.1.1 Method and outcomes.....	31
<b>6. Numerical modelling</b> .....	35
6.1. Introduction to the Finite Element Analysis.....	35
6.2. FEA in biomechanics.....	35
6.3. Biomechanical FEA model generation.....	36

6.3.1	Geometry.....	36
6.3.2	Positioning and orientation of the model.....	37
6.3.3	Materials properties definition.....	38
6.3.4	Contact definition.....	40
6.3.5	Boundary conditions.....	40
6.3.6	Mesh of the model and output request.....	41
6.3.7	Model parameters tuning.....	42
<b>7.</b>	<b>Outputs and comparison between experimental and numerical model.</b>	
	<b>Validation of the test protocol.....</b>	<b>46</b>
7.1	Results.....	46
<b>8.</b>	<b>Conclusion.....</b>	<b>52</b>
	<b>Discussion and future development.....</b>	<b>53</b>
	<b>References</b>	
	<b>Aknowloegment</b>	

## **Abstract**

Knee kinematics is a complex three-dimensional roto-translation movement, which is strongly correlated to the patient anatomy. In particular, the shape of the femurs condyles, the tibia plateau, the patella proximal surface, the morphological and mechanical properties and location of the soft tissue envelope are fundamental to discriminate such movement [1]. For these reasons, each human being has a different knee kinetics and kinematics. Therefore, the understanding of the patient-specific knee joint anatomy and functionality, through dedicated methodologies for kinematic and kinetic analyses and soft tissue mechanical properties determination, is the key factor for closing the gap between surgeons and engineers.

Furthermore, the same techniques can provide useful information regarding the implant of different type of prosthesis, for example the effects of the malpositioning, differences in terms of kinetic and kinematic with respect the native knee [2] or between different implants [3,4,5,6,7].

This project pays attention on a PS TKA implanted knee, developing a complete protocol that describes step by step how is possible linking experimental outcomes with the validation of a FE model, both based on the same specimen.

This could be a start point in better know the difficulties that the validation process may have, giving a possible solution about how better results can be reached and how the kinematics and kinetic trends can be predicted.

## Sommario

La cinematica del ginocchio è un movimento tridimensionale roto-traslatorio complesso, fortemente correlato all'anatomia del paziente. In particolare, la forma dei condili del femore, dei piatti tibiali, della superficie rotulea prossimale, le proprietà morfologiche e meccaniche e la posizione dei tessuti molli sono fondamentali per discriminare tale movimento [1]. Per questi motivi, ogni essere umano ha una cinetica e una cinematica del ginocchio differenti. Di conseguenza, la comprensione dell'anatomia e della funzionalità del ginocchio patient specific, con le metodologie dedicate per le analisi cinematiche e cinetiche e la determinazione di proprietà meccaniche dei tessuti molli è il fattore chiave per eliminare il divario fra chirurghi e ingegneri.

Inoltre, le stesse tecniche chirurgiche si possono rivelare utili nel fornire informazioni riguardo l'impianto di diversi modelli protesici. Sono un esempio lo studio condotto sugli effetti del malposizionamento della componente tibiale o valutazione delle differenze a livello di cinetica e cinematica articolare rispetto al ginocchio nativo [2] o paragonando diverse protesi [3,4,5,6,7].

Questo studio pone la sua attenzione su un impianto PS TKA, sviluppando un protocollo completo che descrive step by step come sia possibile trovare un punto di incontro tra i risultati sperimentali e la validazione di un modello agli elementi finiti, basati entrambi sullo stesso campione.

Questo potrebbe, quindi, essere un punto di inizio in una migliore comprensione delle difficoltà che il processo di validazione può avere, dando una possibile soluzione riguardo a come raggiungere risultati migliori e come predire l'andamento cinematico e cinetico dell'articolazione considerata.

.

# Chapter 1

## Anatomy and Biomechanics of the knee joint

### 1.1 Anatomy of the knee joint

The knee joint is the largest and one of the most complex joints in the human body. A unique interaction of bones, muscles, menisci and ligaments results in a compromise between stability and mobility: the knee has to withstand stresses from body weight and lever forces while at the same time it has to enable mobility to produce movement.

The knee consists of three articulations: two between femur and tibia, the tibio-femoral joints, and one on the anterior side, the patella-femoral joint.

The joint surfaces of the femur, tibia and patella are covered with a thin layer of articular cartilage. The synovial membrane seals the joint and secretes synovial fluid to reduce the friction during movements. The medial and the lateral menisci also have this function and they further act as shock absorbers and pressure distributors.

The knee is a 6 d.o.f. joint which permits flexion and extension as well as limited internal external and abduction adduction rotation and translations in the three directions. The shape of the bones together with the capsule around the knee facilitates these movements.

The bony architecture of the knee consists of two asymmetrical rounded prominences, the femoral condyles (Figure 1.1). The posterior condyles have a circular geometry and are separated by a space called the intercondylar notch. The femoral condyles join anterior and proximally in the femoral trochlear groove. The patella articulates here with the femur. The sulcus is the lowest point of the trochlear groove and lies lateral to the midplane of the distal femur.

The proximal tibia is a tri-dimensional asymmetrical structure (Figure 1.1). The medial articular surface is concave whereas the lateral articular surface is convex. The menisci, which are located on top of the articular surfaces of the tibia, guide the femoral condyles on the tibia surface during flexion and extension.

The patella is the largest sesamoid bone in the body. It is oval shaped and 2-2.5 cm thick. The lateral facet is larger than the medial facet and lies slightly lateral of the femoral midplane. The most important function of the patella is to increase the moment produced by the already strong quadriceps femoris muscle by increasing the lever arm by increasing the distance of the quadriceps tendon from the flexion axis of the knee. The retinaculum and synovium are attached to the patella and the patella tendon and pass around the medial and the lateral aspects of the knee to the distal femur and proximal tibia. The soft tissue sleeve, that runs from hip to ankle, acts

as protector and provides nutritional support to the knee. In addition to skin, fat, capsule and synovium, a network of vessels and nerves is present at the posterior aspect of the knee.

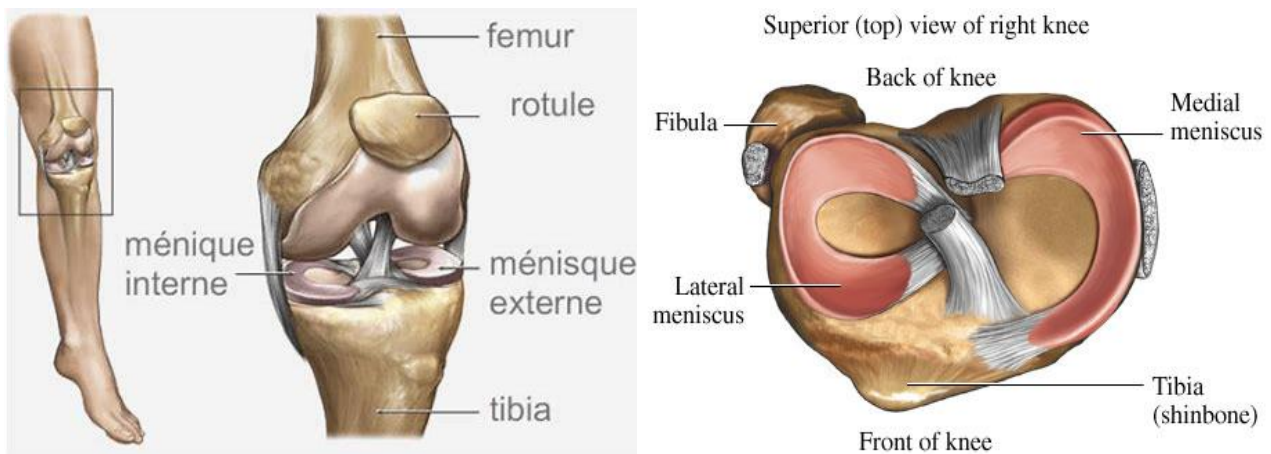


**Figure 1.1:** (left) Bony anatomy of the distal femur and the proximal tibia; (right) Top view of the proximal tibia [Medical Illustration © Nucleus Medical Media, Inc., [www.nucleusinc.com](http://www.nucleusinc.com)]

The major extensor mechanism on the anterior aspect of the knee is formed by the quadriceps (Figure 1.2). This muscle group consists of the rector femoris, vastus lateralis, vastus medialis and the vastus intermedius; it originates from the pelvis (rectus femoris) and proximal femur (vasti) and inserts via the patella tendon to the anterior proximal tibia.

The muscle-tendon complex of the hamstrings, the main knee flexors and the rotators of the knee lie on the posterior aspect of the knee. The lateral hamstring (biceps femoris) and medial hamstring (semitendinosus and semimembranosus) run from the pelvis to the fibular head (biceps femoris) or medial aspect of the tibia (Figure 1.2). Another bi-articular muscle present at the posterior aspect of the knee is the gastrocnemius muscle. This muscle originates proximal and posterior to the femoral condyles and inserts to the calcaneus through the Achille's tendon. The popliteal muscle serves as a static and dynamic posterolateral knee joint stabiliser and runs from the posterolateral femur to the posterolateral tibia and inserts at the Gerde's tubercle.

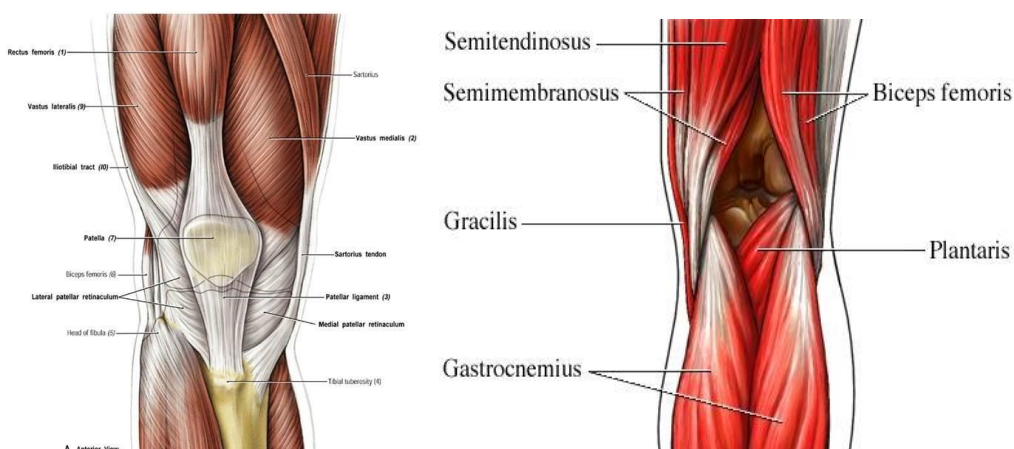


**Figure 1.2:** (left) Quadriceps muscle and tendons around the knee (anterior view); (right) Hamstrings muscle and tendons (posterior view) [Medical Illustration © Nucleus Medical Media, Inc., [www.nucleusinc.com](http://www.nucleusinc.com)]

Four important ligaments join the femur and the tibia: two collateral ligaments and two cruciate ligaments (Figure 1.3). The medial collateral ligament (MCL) consists of the deep and the superficial MCL. The deep MCL originates from the area of the medial epicondyle and inserts on the medial meniscus and the proximal medial tibia plateau. The superficial MCL has the same origin but no meniscal attachment and inserts more distally along the medial tibia. The MCL runs obliquely from posterior proximal to anterior distal.

The lateral collateral ligament (LCL) (Figure 1.3) originates on the femur on the area of the lateral epicondyle and inserts onto the fibula head; opposite to the MCL, the LCL runs obliquely from anterior proximal to posterior distal. The femoral origins of the MCL and the LCL lie on axis through the medial and lateral epicondyle: the epicondylar line.

The anterior cruciate ligament (ACL) (Figure 1.3) originates from the lateral wall of the femoral intercondylar notch and inserts onto the mid-tibia between the articular surfaces. The sagittal slope of the ACL runs from posterior proximally to anterior distally. The ACL is commonly excised during total knee replacement.

The posterior cruciate (PCL) originates from the medial wall of the intercondylar notch and inserts onto the posterior aspect of the tibia (Figure 1.3). the sagittal slope of this ligament is opposite to that of the ACL and runs from anterior proximally to posterior distal.

The origins of the ACL and PCL lie approximately on the axis through the centres of the femoral condyles: the condylar line. The PCL can be either retained or substitute during total knee replacement. The clinical significance of the specific insertions of the four most important ligaments of the knee lies in their ability together with the geometry of the articular surfaces to restrict the laxity of the knee in different flexion angle.

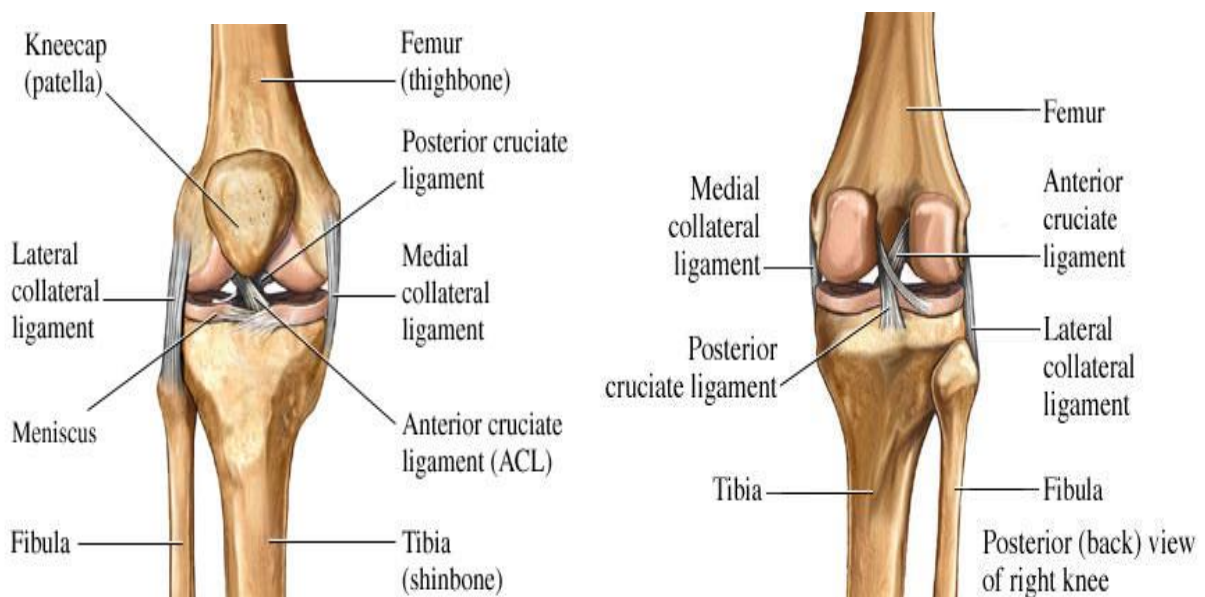


**Figure 1.3:** (left) The ligaments of the knee (anterior view); (right) The ligaments of the knee (posterior view) [Medical Illustration © Nucleus Medical Media, Inc., [www.nucleusinc.com](http://www.nucleusinc.com)]

## 1.2 Biomechanics of the knee joint

### 1.2.1 Kinematics of the knee joint

The complex kinematics of the knee, in terms of tibiofemoral movement, can be fully described by a 'six-degrees-of-freedom' movement with three rotations and three translations along a set of perpendicular axes (the tibial shaft axis, the epicondylar axis and the antero-posterior axis, which is perpendicular to the other axes) (Figure 1.4). The rotational movements are the flexion-extension rotation from 15° to 140°, varus-valgus rotation from -6° to 8° and internal-external rotation from 25° to 30°. The translational movements are the antero-posterior glide between 10-15 mm, the medio-lateral shifting between 2-4mm and the proximal-distal translation between 2-5mm.

Knee flexion/extension involves a combination of rolling and sliding called "femoral roll back" which is an ingenious way of allowing increased range of flexion. Because of asymmetry between the lateral and medial femoral condyles, the lateral condyle rolls a greater distance than the medial condyle during the first 20° of knee flexion from a full extended position. This causes coupled external rotation of the tibia which has been described as the "screw-home mechanism" of the knee which locks the knee into extension guaranteeing stability.

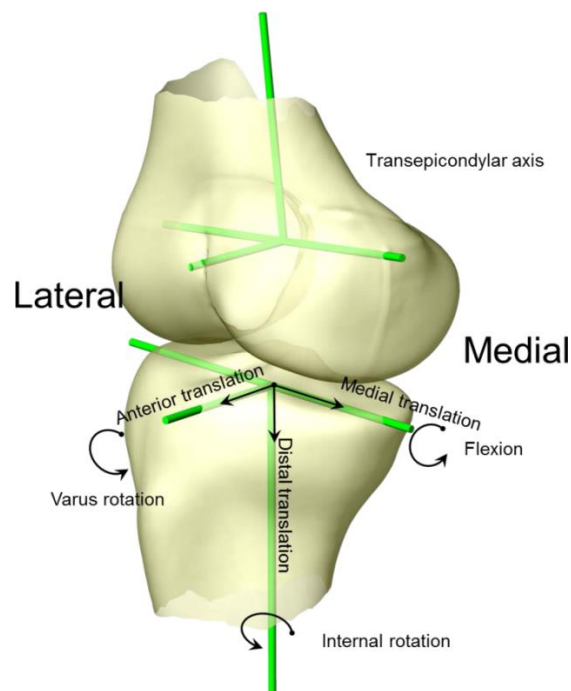


**Figure 1.4:** Diagram illustrating the six degrees of motion of the human knee joint [Medical Illustration © Nucleus Medical Media, Inc., [www.nucleusinc.com](http://www.nucleusinc.com)]

In fact, the flexion-extension movement, from full flexion to full extension, may be described in three phases:

- a) In the fully flexed condition the posterior parts of the femur condyles rest on the corresponding portions of the menisco-tibial surfaces and in this position a slight amount of simple rolling movements is allowed.

- b) During the passage of the limb from the flexed to the extended position a gliding movement is superimposed on the rolling, so that the axis, which at the commencement is represented by a line through the inner and outer condyles of the femur, gradually shifts forward. At this moment of the movement, the posterior two-third of the tibial articular surfaces of the two condyles are involved, and as these have similar curvatures and are parallel to one another, they move forward equally.
- c) Finally, the lateral condyle of the femur is brought almost to rest by the tightening of the anterior cruciate ligament; it moves, however, slightly forward and medial, pushing before it in the anterior part of the lateral meniscus. The tibial surface on the medial condyle is prolonged farther forward than that on the lateral, and this prolongation is directed laterally. When, therefore, the movement forward of the condyles is checked by the ACL, continued muscular action causes the medial condyle, dragging with it the meniscus, to travel backward and medially, thus producing an internal rotation of the thigh on the leg. When the position of full extension is reached the lateral part of the groove on the lateral condyle is pressed against the anterior part of the corresponding meniscus, while the medial part of the groove rests on the articular margin in front of the lateral process of the tibial inter condyloid eminence. The anterior part of the medial meniscus is fitted into the groove on the medial condyle, while the ACL and the articular margin in front of the medial process of the tibial intercondyloid eminence are received into the forepart of the intercondyloid fossa of the femur. This third phase is known as the "the screwing home" or locking movement of the joint.

The movements of the knee joint are determined by the shape of the articular surfaces of the tibia and femur and the orientation of the four major ligaments of the knee joint (MCL, LCL, ACL and PCL).

For the description of the kinematic behaviour of the femur and tibia, relative to each other, the methodology of Grood and Suntay [8] is used to describe the six degrees of freedom.

### **1.2.2 Kinetic of the knee joint**

The knee kinetics consists in the internal stresses that the bones of this joint exchange each other during a dynamic movement.

Previous studies show that the knee joint undergoes a vast range of movements and excessive forces throughout everyday activities. The knee is subject to forces of around four times body weight (BW) during activities such as walking up and down stairs or rising from a chair. Level walking, a necessity to human daily living, exerts compressive forces on the knee in the magnitude of three-four time the BW with this increasing to eight times the BW for downhill walking.

In this study the contact forces, pressures and areas are investigated experimentally using specific sensors and numerically using finite element modelling considering specific region of interest.

# Chapter 2

## Total knee arthroplasty

### 2.1 Introduction

The knee joint has a primary role in all human activities, from daily motions, like walking, sitting, climbing, to 'hard' activities as extreme sports practise (Figure 2.1).



**Figure 2.1:** Some activity examples where the knee joint is directly and essentially involved

The knee joint has to bear very high forces in all human activities, estimated to be even more times the body weight [9], and works for innumerable cycles during the human life. These critical factors can lead to unexpected reduction of the knee joint healthy lifetime, especially in patients with a native not physiologic knee.

If the knee joint turns to be irreparably damaged or worn, a total or partial knee implant is needed.

The most common disease in which a Total Knee Replacement is needed are osteoarthritis, the rheumatoid arthritis and the post-traumatic arthritis [10,11]. All of them are characterized by a damaging of the knee cartilage [12] (Figure 2.2).



**Figure 2.2:** Osteoarthritic knee. The degradation of the cartilage is combined to osteophytes growth on the knee joint surfaces.

## 2.2 TKA components

The Total Knee Arthroplasty (TKA) is a surgical operation in which the entire knee joint is replaced using an artificial device (Figure 2.3).



**Figure 2.3:** Knee joint after TKA implant

TKA is usually made by four components, when also patella is resurfaced (Figure 2.4). The femoral component replaces the damaged femoral cartilage whereas the tibial insert and tibial tray replace the menisci and the tibial articular cartilage.

The femoral component is generally made in metal, like Chrome-Cobalt alloy. The tibial tray is generally made in metal, like Titanium [13,14], whereas the tibial insert is made by Ultra High

Molecular Weight Polyethylene (HUMWP), tuned to be in contact with metallic femoral component reducing wear, debris formation and augmenting prosthesis lifetime [15]. Many studies have been reported in literature in which the materials are compared in terms of wear and performance in TKA application [16].

The patellar component replaces the posterior surface of the patellar bone, the part that gets in contact with the femoral component. This component is not always replaced because of the high risk of loosening and infection it leads, thus resurfacing of the patella rests with the surgeon [17,18,19].



Figure 2.4: TKA components

### 2.3 TKA standard design implant

The aim of TKA is to replace the damaged knee joint surfaces, thus the surgeon removes the distal part of the femur and the proximal part of the tibia in order to not change significantly the dimension and the physiologic alignment of the knee [20,21] (Figure 2.5).

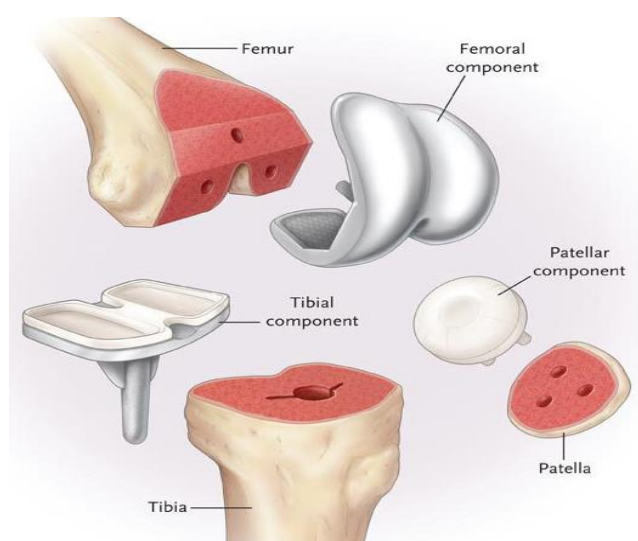


Figure 2.5: TKA implant. Femur, tibia and patella after bone resection. The damaged joint is completely removed. The TKA is performed with the removed parts replace by TKA components.

For this purpose the surgeon resects the tibial and the femur bone among several resection planes, identified according to the position of specific anatomical landmarks and the TKA design in use [22,23].

The tibial resection is monoplanar and comprehends and hole fitting the tibial tray stem whereas the femur resection consists of several cutting planes fitting the several internal faces of the femur component [24].

There are several guidelines developed to achieve a physiologic alignment of the TKA in the knee joint.

The most diffused theory for a correct alignment was introduced by Insall et All [25]. It provides the tibial and femoral resection planes to be perpendicular to the mechanical axes of the tibia and femur as collinear and vertical. Normally, in absence of tibial deformity, the anatomical and mechanical tibial axis are coincident [26].

Thus, the identification of the mechanical axis of the femur and the mechanical or anatomical axis of tibia bone, sometimes also joined with the use of a computer-assisted navigation system to place the cutting tool consequently, allows the surgeon to achieve a frontal correct alignment of the knee in TKA [27] (Figure 2.6).



**Figure 2.6:** Example of a computer-assisted new technology by Smith & Nephew to provide cutting guide to the surgeon.

# Chapter 3

## Aim of the study

### 3.1 Introduction to the analysis

#### 3.1.1 State of art and background

In the last years, several studies were performed using robotic simulator [28,29] showing how different technique could be beneficially used to investigate accurately knee joint kinematics, in terms of both rotations and translation. Furthermore, the coupling of numerical analysis to experimental activity [30] show big improvement in the results, allowing sensitivity analysis, providing accurate information on contact force and pressure [31], investigate bone stress, or integrating with additional outcomes as risk of fracture or ligament strain distribution [32].

Experimental evidence showed that the kinematic and kinetic knee joint activity is highly patient dependent, both in healthy and in patient with prosthesis, moreover, a wrong position of the implant or a bad choice of the soft tissue position during modelling could induce high alteration of the joint forces (up to 60%) even if the change in kinematics could be quite small (less than 5% compared with the theoretical position) [33]. Experimental techniques combined to numerical ones showed that a close to real model of the knee joint is fundamental. Moreover, especially in analysing patient with knee prosthesis, results of several study highlight how kinematics is not the only and also not the most relevant parameter to predict or explain knee function but knee kinetics should be integrated in the clinical follow-up [34].

Dedicated patient-specific experimental and numerical methodologies showed to be the promising tool to fill this gap surgeon and engineer and to guide patients from immobility to mobility, overstepping their disease.

In the following chapters the protocol proposed for the validation of the PS TKA FE model is deeply described.

#### 3.1.2 Workflow and Research questions

The project is sub-divided into three main pillars (Figure 3.1):

- a) Kinematic tests on cadaveric specimens;
- b) Constitutive modelling of the soft tissues of the knee envelope;
- c) Development and validation of the FEA models.

In the first step (a), one cadaver leg is tested on passive movement in order to collect the patient specific kinematic and kinetic after TKA implant.

Secondly (b), the lateral collateral ligament (LCL) and the medial collateral ligament (MCL) are collected from the specimen used for the experimental passive movement. They are tested in a tensile machine in order to obtain the patient specific mechanical properties of soft tissues. Following this approach, the behaviour of the soft-tissues can be verified.

Once the material models and properties of the main soft tissues are determined, using the donor CT and MRI scan images, the patient-specific FE model of all the main structures of the knee is developed (c). The outcomes collected are kinematic, contact areas, contact pressures and contact forces in specific regions of interest.

The validation of the protocol consists on the comparison of the experimental outcomes with the numerical ones obtained. Eventual model tuning can be performed in order to best fit the model behaviour with the experimental findings.

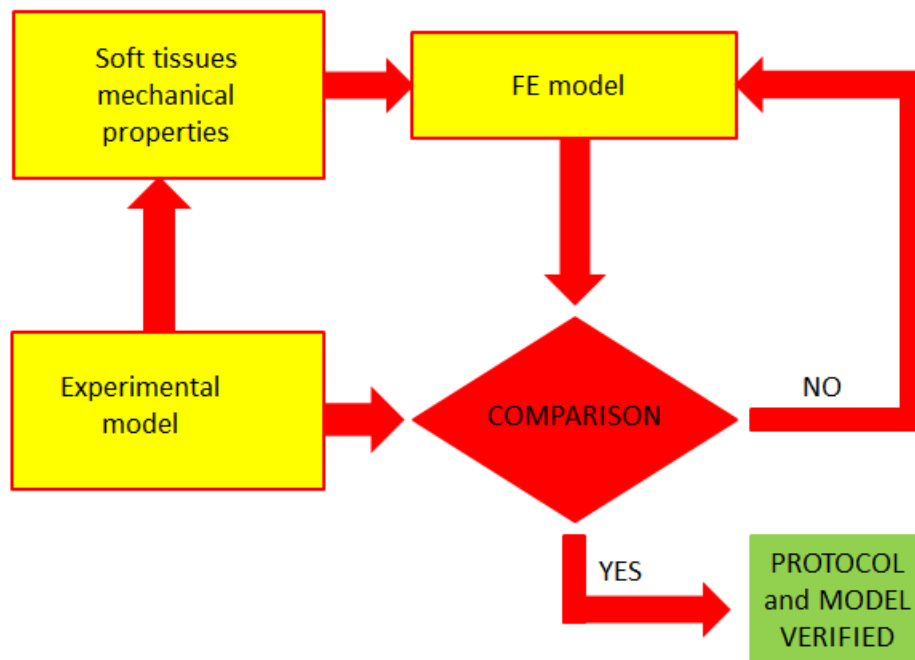


**Figure 3.1:** Workflow of the activity

# Chapter 4

## Experimental test

### 4.1 Pilot tests and protocol difficulties

Four cadaver legs were tested before the final simulation in order to better know the difficulties involved in this procedure. During, in fact, the previous tests the following critical points have been identified:

- a) The selection of a specimen without previous implant, in order to implant the prosthesis in a native knee. Could be better also choose a cadaver leg without any dysfunction (ex. hip damaging, high osteoporotic bones, small contact surfaces);
- b) The guides used to cut and position the specimen in the boxes used during the simulation have to be calculate on the STL bone surface. It is really important that the bone surface is not smoothed too much on segmentation software. That may lead to have a smaller cutting guide that does not fit on the specific bone on which was modelled;
- c) The test is highly dependent on the time: the more is the simulation time, the higher will be the laxity of the soft tissues. In this analysis is really important to maintain the strength of the medial and lateral collateral ligaments;
- d) The placement of the different marker sets of femur and tibia during the CT scan is helpful to the orientation of the Fe model in the same reference system of the motion capture system;
- e) The positioning of the Tekscan sensors in order to estimate contact areas, forces and pressures in the tibio-femoral joint should not be underestimated. Furthermore, a small tibio-femoral joint may not allow a completely flat surface of the sensor and can lead to measurement of meaningless data (Figure 4.1);
- f) Tekscan sensors positioning with suture shows worst result than position them without suture (Figure 4.1);
- g) The synchronization of all the measuring systems involved in the tests is really important in order to correlate each sensor data acquisition to a precise angle of the flexion-extension movement. Without the synchronization is not possible to know which is the internal force involved in different precise angles of the movement.

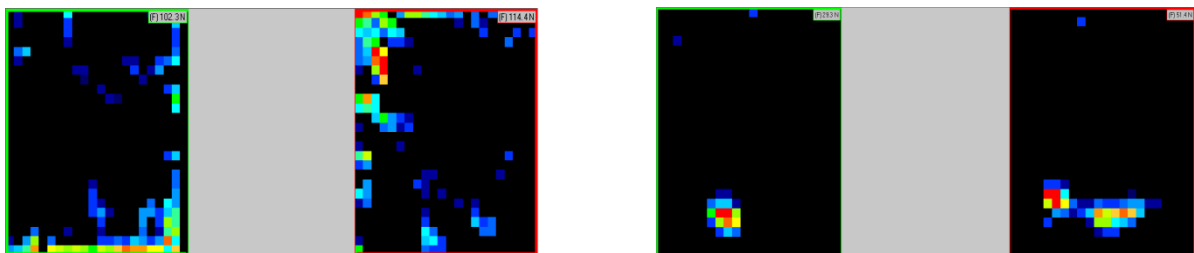


**Figure 4.1:** (left) Useless measurements of contact forces; (right) Usefull measurements of contact forces. Both in the tibio-femoral joint.

The following chapter, anyway, will present the entire procedure applied solving any doubts on the previous analysis on difficulties involved on it. The procedure was developed following previous studies [35].

## 4.2 Final test: definition of a complete experimental protocol during passive movement of implanted knee

### 4.2.1 Methodological sequence

Five fresh frozen cadaver specimens were used for the ex vivo testing, four for the pilot experiments as said previously and one for the subsequent measurement. The ex vivo experimental set-up was guided by the following sequence. A description of all steps is given.

#### 4.2.1.1 Preparation of the test

The preparation of the test consists in different step, explained as follows:

a) **CT scanning of frozen specimen and segmentation of CT scan images**

The specimen consists of a complete limb, disarticulated at the level of the hip, which has been fresh frozen. The specimen was transported in frozen state in an isolating box to the CT scan. For the cadaveric knee specimen, we obtained volumetric CT scans on a 64-row helical multidetector computed tomography (MDCT) scanner (General Electric Lightspeed VCT, Milwaukee, WI). The images were obtained at 120 kV and 450 mA, with a slice thickness of 1.25 mm and a pitch of 0.5 mm/rev (Figure 4.2). Raw data were processed using a bone filter. The images were stored in DICOM format onto a USB port. The CT scans were analysed using ScanIP® (Simpleware, Synopsys, Exeter, UK) to create the surface reconstruction and identify the bony landmarks [36].



**Figure 4.2:** MRI scan of the specimen.

**b) 3D printed custom-made guides for controlled alignment and cutting in biomechanics test**

The surface reconstruction was used to obtain different alignment and cutting blocks [37], for an accurate positioning in the potting of distal femur and proximal tibia with respect to the testing advice (Figure 4.3).

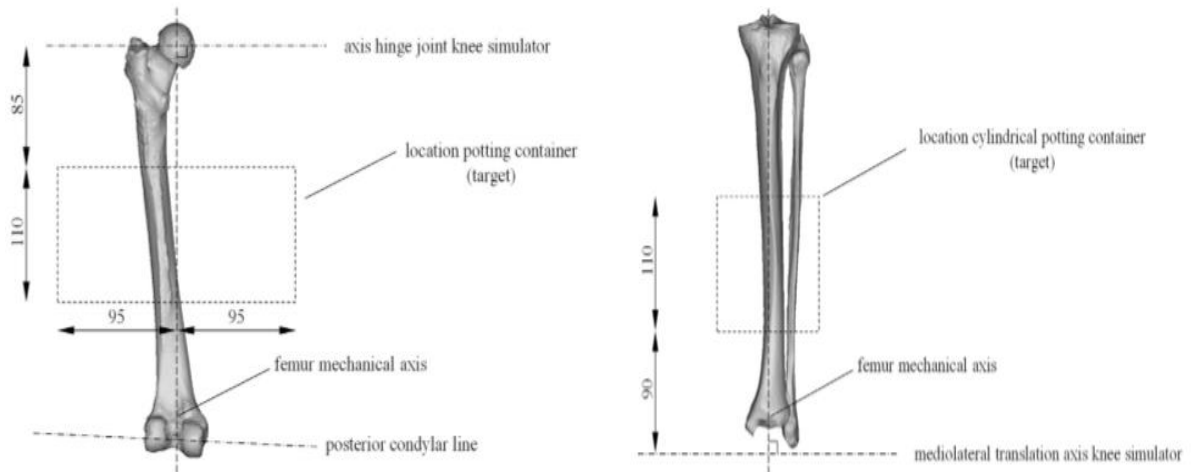


**Figure 4.3:** Schematic boundary condition for femoral (a) and tibial (b) fixation.

To obtain these boxes were needed the landmarks registration on the CT scans in order to align standard boxes on the femur and tibia in the way that the bone was completely covered by the guides. We used Matlab® (Mathworks) for the alignment (Figure 4.4).

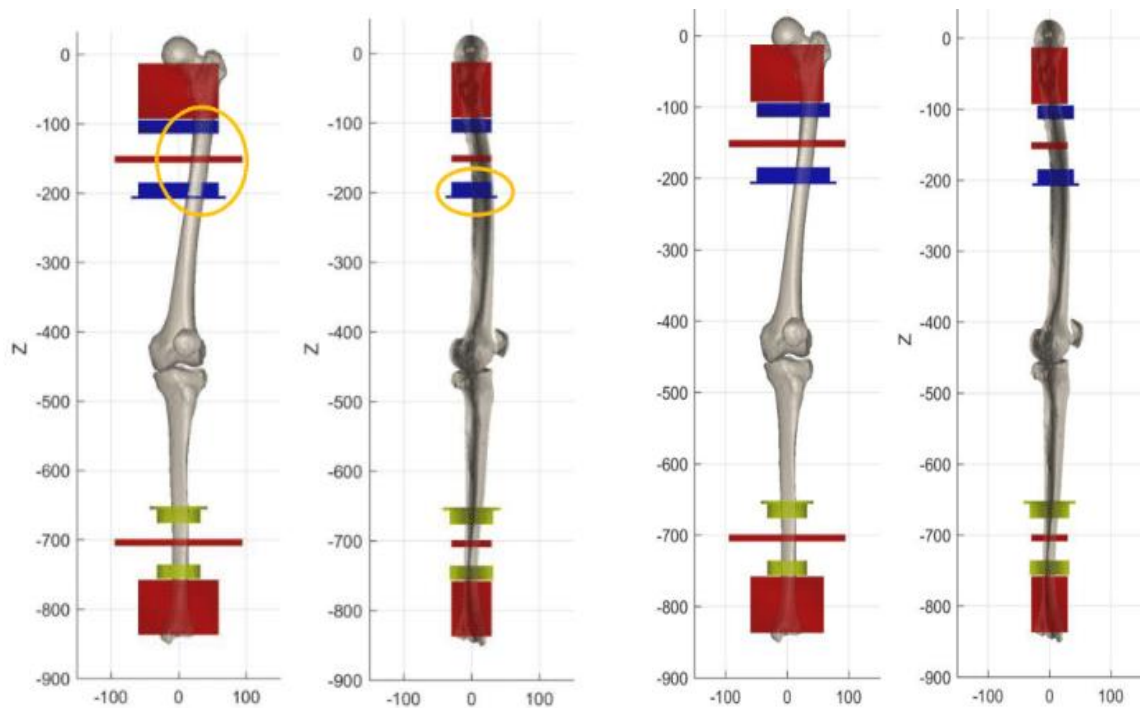


**Figure 4.4:** (left) Bad alignment of the guides; (right) Repositioning of the guides in order to completely covered the bone.

Later we used Mimics software in order to subtract the bone from the alignment and cutting guide using the Boolean function (Figure 4.5-6).

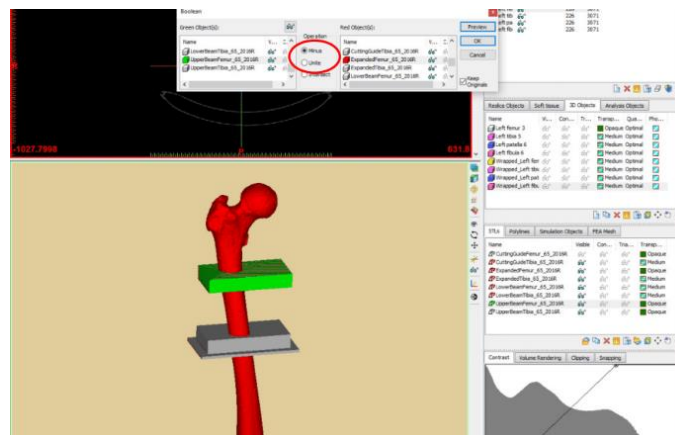


**Figure 4.5:** Subtraction of the bone from the cutting and alignment guides of femur.

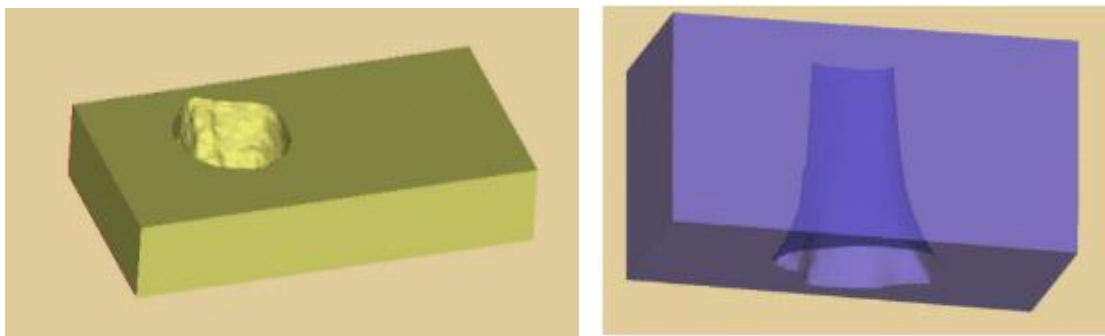


**Figure 4.6:** Femur and tibia cutting guides.

Using SolidWorks (Dassault systems) the final design of the alignment and cutting guide was made. Using the six guides from which the bone was subtracted, we needed to remove the excess material.

With regard to the alignment guide, we split them in two parts, which were assembled back by means of lock mechanism. In addition, extra cavities were created to remove excess material and allow the resin used to fix the bones in the boxes to enter. (Figure 4.7).

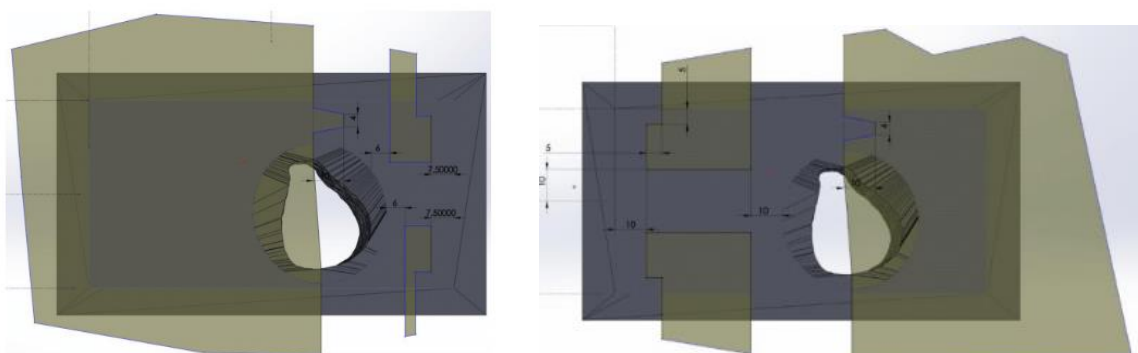


**Figure 4.7:** Design of femur alignment guide: splitting in two parts with lock mechanism.

With regard to cutting guide, the blocks were cut in order to allow the fitting of the bones inside and permit the removing of the excess bony material (Figure 4.8).

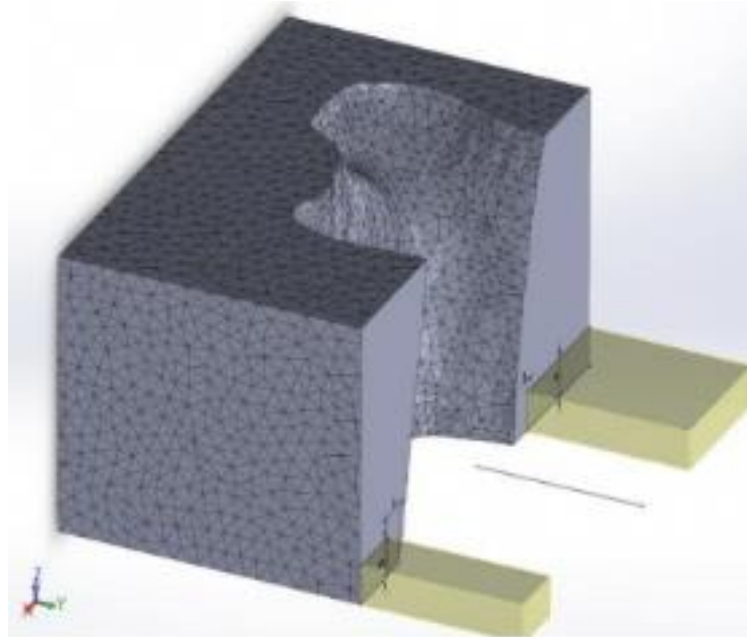


**Figure 4.8:** Design of the femur cutting guide.

All the 3D printed alignment and cutting guides are shown in the following figure (Figure 4.9).



**Figure 4.9:** 3D printing of the final design of the alignment and cutting guides for femur and tibia.

**c) Thawing of the specimen**

Two days before the experiment, the specimen was taken out of the refrigerator to allow 48 hours for thawing.

**d) Tekscan sensors calibration**

Tekscan sensors were used to quantify the interaction between the prosthesis components. Tekscan is a matrix-based pressure sensing system, where each sensor element has an area of 1,67 mm<sup>2</sup> organised in two matrixes of 26 rows and 22 columns

(Figure 4.10). The sensor consists in two silver conductive layers fixed on flexible substrate. One conductive layer forms a row pattern while the other a column pattern. When they are superimposed they form a matrix pattern. Between the conductive layers a semi conductive material is interposed.

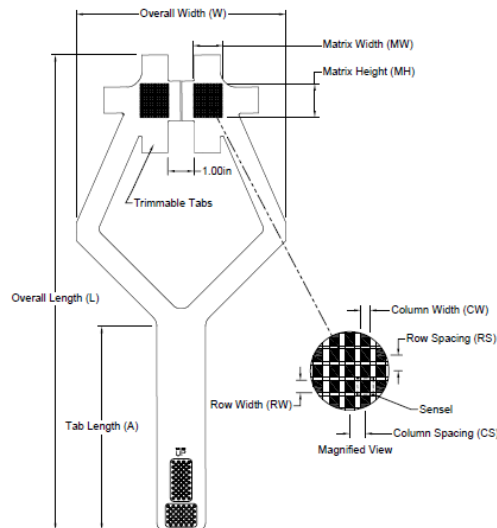


**Figure 4.10:** Design of the Tekscan sensor used in this study.

When a pressure is applied on a cell electric resistance changes. Scanning periodically all the cells it is possible to reconstruct the pressure distribution on the entire sensor surface. The following figure shows a simple electronic scheme of the acquisition method and sensors structure (Figure 4.11).

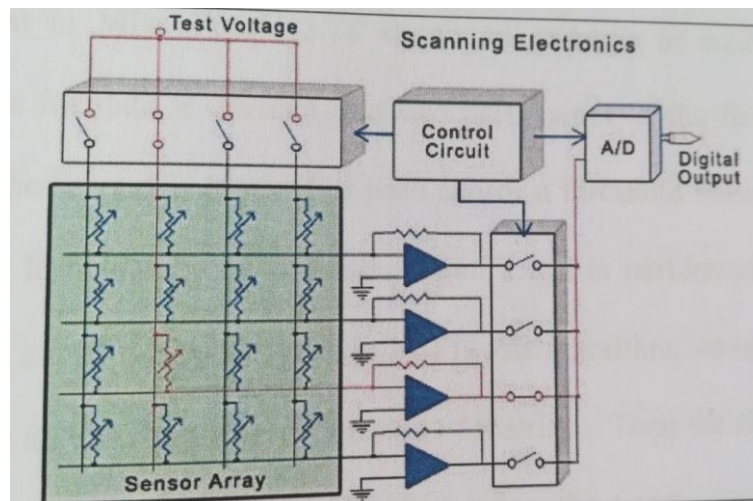


**Figure 4.11:** Tekscan electronic scheme.

Maximum acquisition rate is 100 Hz, depending on the operator's need. Data acquired is elaborated by the Tekscan software (I-scan) and can be saved in ASCII format. Before using, each sensor needs to be calibrated [38]. To obtain a more accurate calibration, a calibration protocol was developed using the loading frame, whose control software permits to create a loading sequence.

The sensor was fixed between two rectified metal blocks (Figure 4.12).

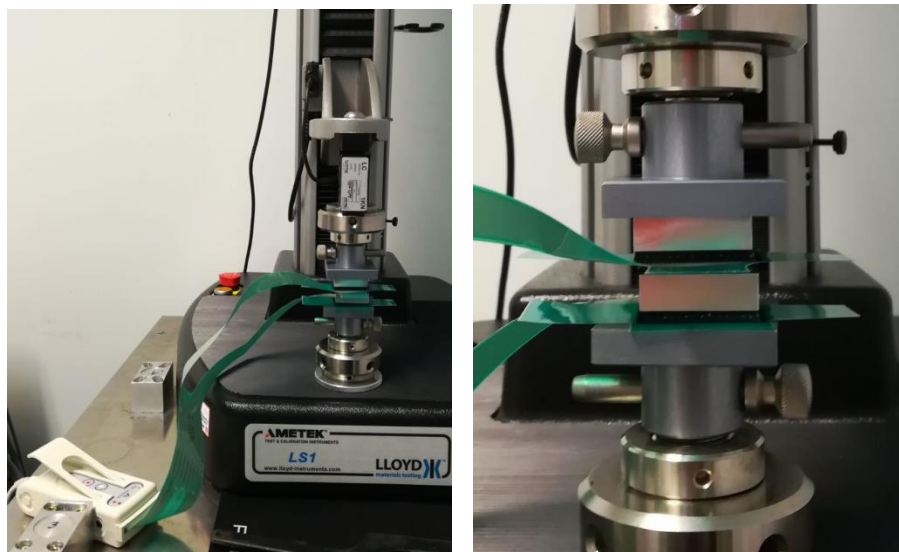


**Figure 4.12:** (left) Tekscan reader and sensor positioned in the loading frame; (right) metal blocks placed between the two surfaces of the sensor.

Loads were applied from 100 N to 750N, with intervals from 100 N to 150N. Forces were maintained for 30 seconds, to permit the controller of the loading frame to reach higher level of precision and the results recorded with I-scan software. The output file is a series of matrixes containing the map of the sensor, with a number of frames depending on the acquisition rate chosen. Each element has value from 0 to 255 and can also represent the pixel values of an image. For each load the mean values of all the matrixes are calculated and the sum of all the cells is obtained. The sum is multiplied by the area of a single cell, then divided by the total area. That is the number of cells activated multiplied by the area of a single cell. The load applied is also divided by the area of the single cell. The results for all the loads are plotted on a graph, that represent the relation on the value of a single pixel with the pressure expressed in MPa (Figure 4.13).

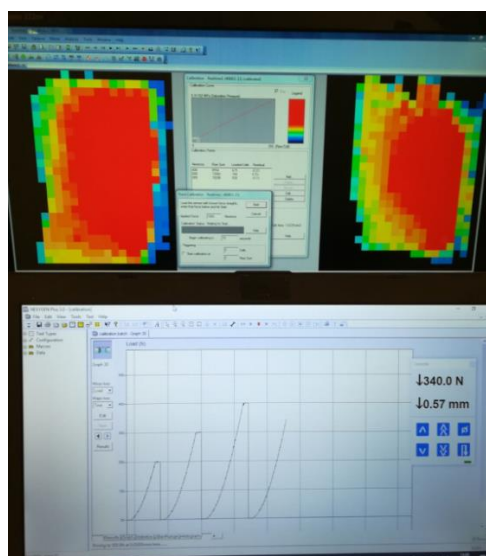


**Figure 4.13:** (top view) I-scan software shows the contact force applied with a color map; (bottom view) The curve shows the loads applied by the loading frame in the meantime.

The following figure shows one of the multiple sensors calibration curves (Figure 4.14).

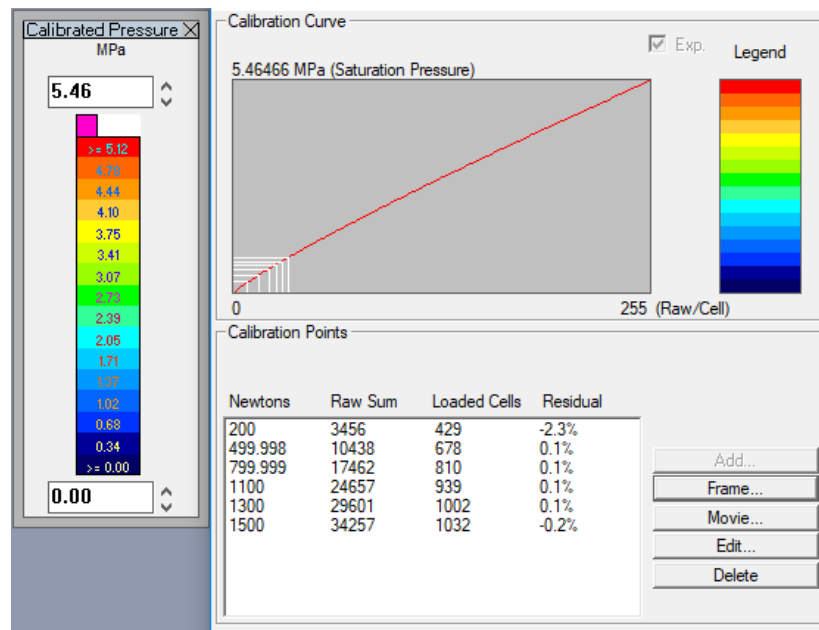


**Figure 4.14:** Tekscan calibration curve.

When a test is performed with the Tekscan sensor, the calibration curve is applied using I-scan software, which opens the ASCII files and organizes all the frames in a structure of matrixes. Than for all the pixels of each frame the correct pressure value is calculated using appropriate calibration curve. The force value is obtained calculating the area where the load is applied in  $\text{mm}^2$  and multiplying by the pressure value.

**e) Optitrack motion capture calibration, rigid body creation of marker sets and pointer**

Four cameras were positioned on the medial side of the specimen to allow maximal visualization of the optical reference markers fixed to the tibia and femur. Using a special want with calibrated distance between the reflective spheres, the software was instructed to calculate the relative position of the cameras in space (Figure 4.15).



**Figure 4.15:** (left)Cameras positioning before the calibration process; (right) Calibration process.

Successively 3 rigid body were created of the Y-shaped markerset of femur, T-shaped markerset of tibia and of the pointer used to identify in the next step the bony landmarks (Figure 4.16).

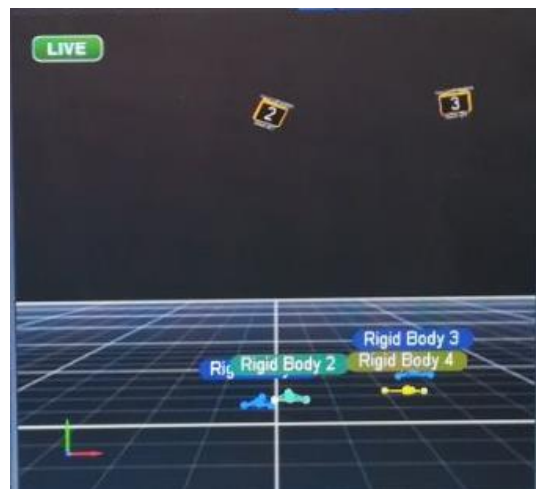


**Figure 4.16:** Rigid body initialisation. This picture shows four rigid body due to the fact that the patella was taking in account for a following active test.

**f) Preparation of the specimen**

The fat tissue was removed by the surgeon in order to have soft tissues in the proximal volume of the knee joint (Figure 4.17).



**Figure 4.17:** (top) Cadaver specimen before the excess tissues removing; (bottom) Specimen without useless tissues.

Successively the markersets were fixed on the femur and tibia and different landmark points in regions of interest were collected (ex. Hip neck, femur bone surface, landmarks of femur and tibia) using the pointer markerset (Figure 4.18).



**Figure 4.18:** Tibial ankle center (TAC) registered using the pointer.

Using the cutting guide the excessive bone in proximal femur and ankle was removed. Using the alignment guide the tibia and the femur were fixed in the containers with polymethylmethacrylate (PMMA). Screws were driven into the end of the bones for providing sufficient rotational control in the PMMA (Figure 4.19-20).

Finally, the PS TKA implant was implanted and the Tekscan sensor placed without any suture in the tibio-femoral joint (Figure 4.21).



**Figure 4.19:** (top) cutting blocks positioning; (bottom) Ankle and femur head removing.

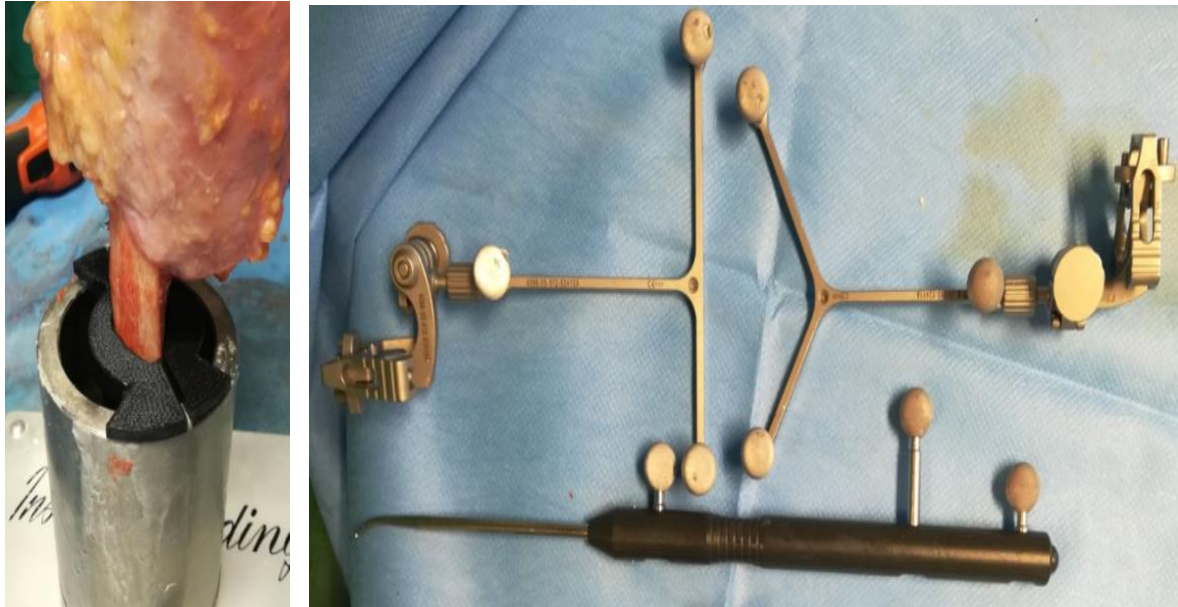


**Figure 4.20:** (left) Tibia into the container with the alignment guide; (right) Markersets of tibia (T), femur (Y) and pointer.

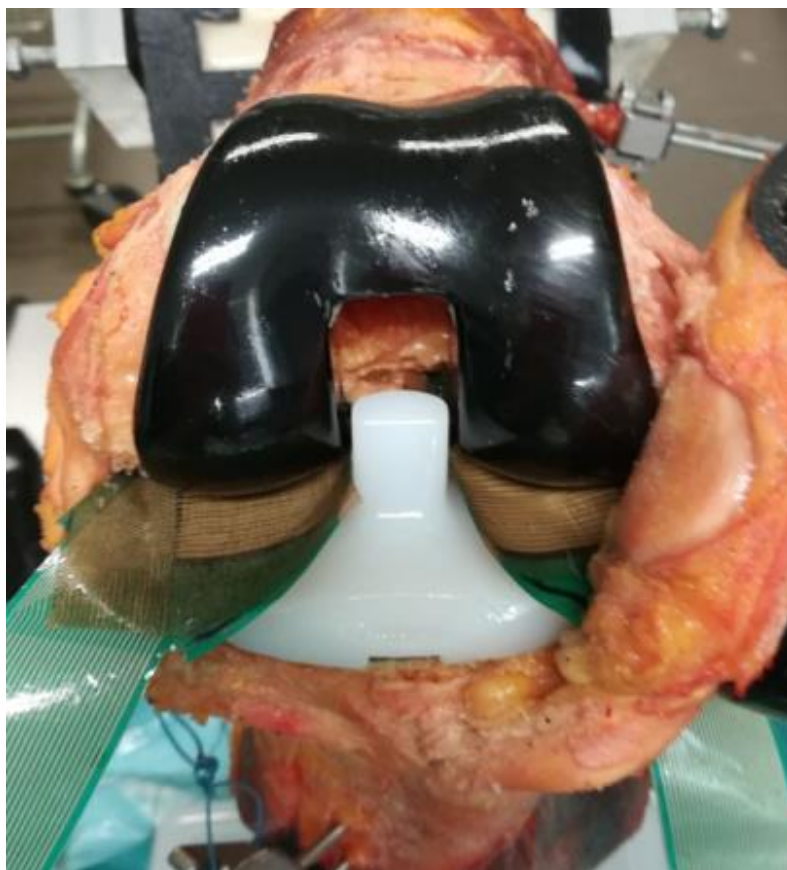


**Figure 4.21:** Implant of the prosthesis and placement of Tekscan sensor.

**g) Mounting of the specimen in the Oxford rig**

The specimen was then mounted onto the mechanical knee rig with the containers rigidly fixed to the hip actuator and the ankle load cell (Figure 4.22).

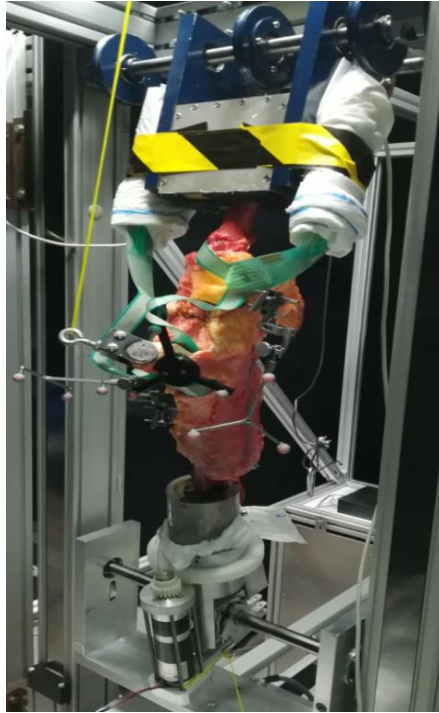


**Figure 4.22:** Positioning of the specimen in the Oxford rig.

#### 4.2.2 Passive test and kinematic real time measurement

The position of the rigid bodies consisting of the femur and tibia, with their respective reference frames, was followed as a function of time by the 3D motion analysis system. The loads were measured with calibrated load cells. Initial recording consisted of a positioning of the knee in full extension with the tibial container fixture loose along the vertical axis. The knee was then pulled into full extension. Static recording of the position of the rigid bodies was performed. The knee was then initialized at a position of 20° to 30° of flexion for starting the dynamic measurements. A squat was performed (Figure 4.23) and motion and loads were recorded during the full cycle. The full set of measurements was performed without any load applied on the hamstrings or quadriceps.

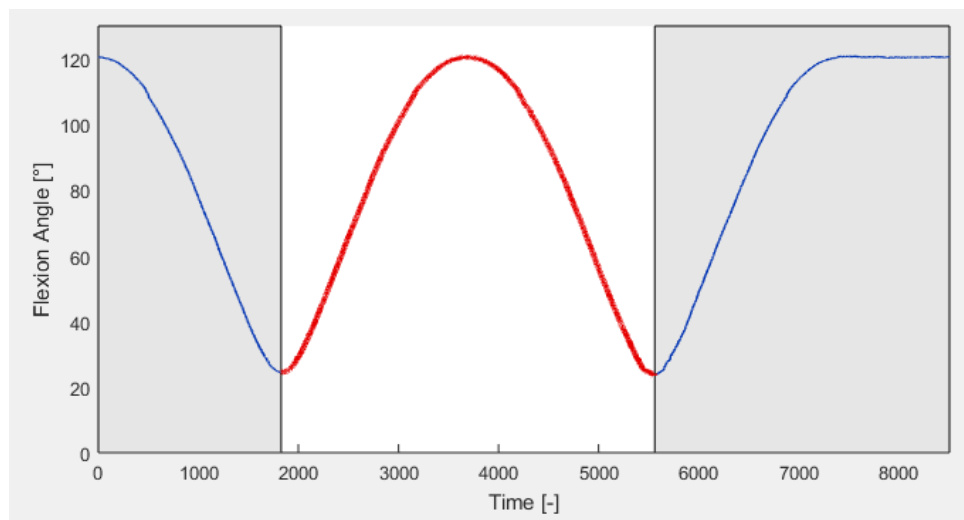


**Figure 4.23:** Squat movement. The blue curve represents all the cycles performed. The red underlined curve represents the effective flexion-extension movement recorded.

The kinematic was quantitatively estimate real time during the test using the Grood and Suntay reference system for femur and tibia [39]. The relative motion between the two bodies in time was thus defined by the change of the relative position of their coordinate systems. This joint motion is described by six degrees of freedom. The coordinate system of each body was defined by means of four reference point, collected during the preparation of the specimen (Table 4.1).

Points	Femur	Tibia
p1	Femoral Hip Center (FHC)	Tibial Knee Center (TKC)
p2	Femoral Knee Center (FKC)	Tibial Ankle Center (TAC)
p3	Femoral Medial Condyle Center (FMCC)	Tibial Medial Condyle Center (TMCC)
p4	Femoral Lateral Condyle Center (FLCC)	Tibial Lateral Condyle Center (TLCC)

**Table 4.1:** The anatomical reference points for femur and tibia used to create a Cartesian system for each body.

The axes of the Cartesian coordinate system are called the medio-lateral axis, antero-posterior axis and mechanical axis, which were calculated according to the following equations.

$$\text{Mechanical axis} = \frac{p1-p2}{||p1-p2||} \quad (4.1)$$

$$\text{Antero – posterior axis} = (\text{Mechanical axis}) \times \frac{p3-p4}{||p3-p4||} \quad (4.2)$$

$$\text{Medio – lateral axis} = (\text{Antero – posterior axis}) \times (\text{Mechanical axis}) \quad (4.3)$$

Substituting the coordinates of the anatomical reference point. Shown in Table 4.1, in Eq. (4.1), (4.2) and (4.3), the Cartesian Coordinate system for tibia and femur were given. The medio-lateral axis, antero-posterior axis and mechanical axis were the defined as *i*, *j*, and *k* for the tibia and as *I*, *J* and *K* for the femur. The origin of the femoral and tibial coordinate system was chosen at the medial side, p3.

The previously derived Cartesian coordinate systems are coordinate systems fixed to femur and tibia (Figure 4.24). In order to describe the relative motion between femur and tibia, a joint coordinate system id derived.

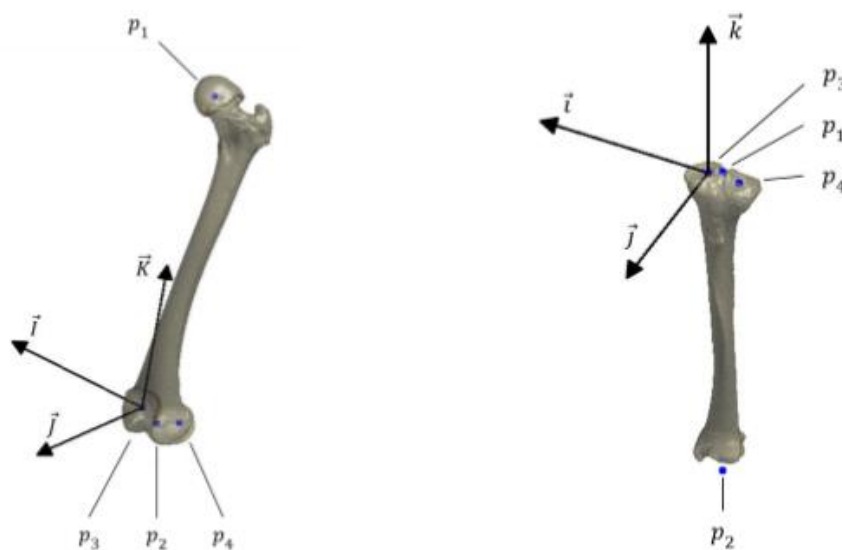


**Figure 4.24:** Visualization of the anatomical reference points together with the resulting Cartesian coordinate system of femur (left) and tibia (right), with origin in p3.

Either the femur or tibia coordinate system is chosen as reference and is set fixed at the origin. The choice is important for the sign convention and must hence be taken in account during the calculations. For a coordinate system describing the motion of the femur relative to the fixed tibia, the joint coordinate system is derived according to the following equations.

$$\text{Medio – lateral axis:} \quad e_1 = I \quad (4.4)$$

$$\text{Antero – posterior axis:} \quad e_2 = e_3 \times e_1 \quad (4.5)$$

$$\text{Medio – lateral axis:} \quad e_3 = k \quad (4.6)$$

The joint coordinate system consists out of two fixed axes ( $e_1$ ,  $e_3$ ) and one floating axis ( $e_2$ ), respectively the medio-lateral axis of the femur, the mechanical axis of the tibia and the cross product of both. The axes are chosen in that way that flexion-extension occurs about the femoral fixed axis ( $I$ ), internal-external rotation about the tibial fixed axis ( $k$ ) and valgus-varus about the floating axis ( $e_2$ ) (Figure 4.25).

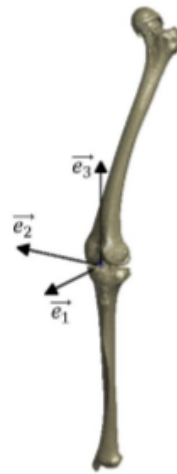


**Figure 4.25:** Visualization of the femoral-tibial joint coordinate system, with origin in p3.

Flexion-extension ( $\alpha$ ) is defined as the angle formed between the floating axis ( $e_2$ ) and the femoral anterior axis ( $J$ ). The relation given by Eq. (4.7) is used to obtain the magnitude of  $\alpha$ .

$$\cos(\alpha) = J \cdot e_2 \quad (4.7)$$

Since  $\cos(\alpha) = \cos(-\alpha)$ , a sign correction has to be applied for  $\alpha$  when the following inequality is satisfied.

$$\sin(\alpha) = e_2 \cdot K > 0 \rightarrow \cos(-\alpha) = J \cdot e_2 \quad (4.8)$$

Internal-external rotation ( $\gamma$ ) is defined as the angle formed between the floating axis ( $e_2$ ) and the tibial anterior axis  $j$ .

$$\sin(\gamma) = e_2 \cdot i \quad (4.9)$$

The valgus-varus angle ( $\beta$ ), computed by Eq. (4.10), is obtained from the angle between the tibial and femoral body fixed axes.

$$\cos(\mu) = I \cdot K \rightarrow \beta = \mu - \frac{\pi}{2} \quad (4.10)$$

The three translations are computed by subtraction of the position of origin of the tibia from the position of origin of the femur and projecting the resulting vector on each axis of the joint coordinate system. That is given by the following Eq. (4.11).

$$\begin{aligned}
 H_{medial} &= (p3)_{tibia} - (p3)_{femur} \\
 q1,_{medial} &= H_{medial} \cdot e1 \\
 q2,_{medial} &= H_{medial} \cdot e2 \\
 q3,_{medial} &= -H_{medial} \cdot e3
 \end{aligned} \tag{4.11}$$

The resulting translations are the medio-lateral ( $q1$ ), anterior-posterior ( $q2$ ) and distraction-compression translation ( $q3$ ) for the medial side of the bone. These translations can also be calculated for the lateral side, this by choosing as origin  $p4$  in the Cartesian coordinate systems of femur and tibia. The translations are then given by the following Eq. (4.12).

$$\begin{aligned}
 H_{lateral} &= (p4)_{tibia} - (p4)_{femur} \\
 q1,_{lateral} &= H_{lateral} \cdot e1 \\
 q2,_{lateral} &= H_{lateral} \cdot e2 \\
 q3,_{lateral} &= -H_{lateral} \cdot e3
 \end{aligned} \tag{4.12}$$

Furthermore, the kinetic was also measure real time positioning the Tekscan sensor in the knee joint during the flexion-extension movement.

In Chapter 7 all the outcomes will be presented and compare to the numerical results.

# Chapter 5

## Mechanical characterization of MCL and LCL

### 5.1 Tensile test

In an intact human joint, the soft-tissues that are involved differently act to provide joint stability and to transmit movement and forces. Unfortunately, when searching on the literature, no unique behaviour can be found in response on a search of a specific soft tissue. The difficulties in defining the correct material behaviour, in term of material model and properties, can be attributed to the fact that mechanical characteristics vary significantly from one person to another. In this project a mechanical uniaxial tensile test was chosen to determinate the MCL and LCL patient specific mechanical properties. This experimental procedure permits to calculate the Young's modulus and the Poisson ratio for a soft material characterized by a tensile test [40].

#### 5.1.2 Methods and outcomes

The testing protocol consists in characterising a specimen by using a tensile uniaxial test and an automatic contactless procedure. The tensile machine used for this project is the LS1 AMETEK Lloyd instruments universal testing machine coupled with a load cell of 1 kN. Sampling frequency was 1000 Hz. Nexygen plus, a data analysis and material testing software developed by AMETEK Lloyd instruments, is the interface between the tensile machine and the user.

In order to avoid potential sliding between the specimen and the clamps of the machine during the test, several markers were drawn directly on the specimen (Figure 5.1). The marker thus allows to measure the true displacement of the material even in different regions of interest. A camera with fixed position and previously calibrated is used to record the test and provide frames to a tailored algorithm that recognizes the contour of markers. The camera fixed on an adjustable shelf must be perfectly aligned to the vertical plane where the specimen will be stretched. For an acquisition device, the resolution is related to the number of pixels  $r = N_x \times N_y$  contained in an image, but even to the original image area  $A$  that can be captured by the camera. Indeed, the effective resolution can be defined as  $R = r/A$ .

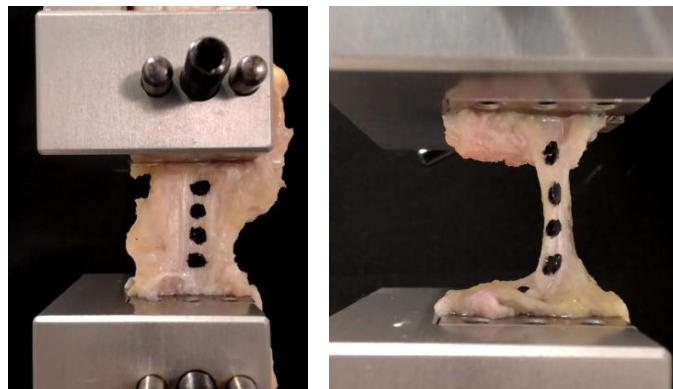
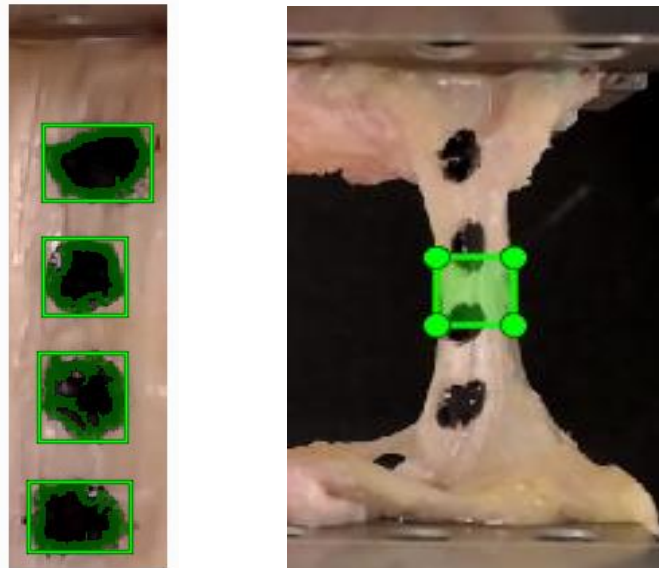


Figure 5.1: MCL (left) and LCL (right) markers positioning.

Special care needed to be taken that the camera records all the surface of the specimen during the whole test. The camera was set in order to define as well as possible the contour of markers and the perimeter of the specimen. In fact, even small objects of the image, as for instance the surface of markers, should be quite defined and described by an enough number of pixel for being accurately tracked by the imaging algorithm. It follows that accurate results strictly depend on a right distance choice between camera and specimen.

In post processing, the image analysis allowed to calculate the markers displacement and the mean width variation of the specimen. The post-processing of the images was done using ICY open source software.

At the beginning the images needed to be cut considering only the region where markers were placed. Using the crop images, the markers were recognised by size parameters and threshold upper and lower limits. To estimate the width a similar protocol was used but the region considered was a central portion of the ligaments compared to the black background. The width variation of the green box in the following figure was assumed the same of the width variation of the ligament (Figure 5.2). The force data and load frames needed to be insert.



**Figure 5.2:** (left) MCL markers detection; (right) LCL width estimation.

Through the true displacement variation, it was possible to obtain the true strain  $\epsilon_l$  of the material:

$$\epsilon_l = \ln[L(t)/L_0] \text{ [Adimensional]} \quad (5.1)$$

Where  $L(t)$  is the instantaneous longitudinal distance between two markers and  $L_0$  is the initial distance between two markers.

During the stretching of the specimen, its cross-sectional area varies. As simplifying assumption, the thickness was assumed constant, but using a black and white threshold imaging technique it was possible to estimate the specimen mean width variation (Figure 5.2).

Markers and background must be brighter or darker than the colour of the specimen surface. Through the estimate of cross sectional area variation, it is possible to obtain the true stress of the material:

$$\sigma = F(t)/A(t) \text{ [MPa]} \quad (5.2)$$

Where  $F(t)$  is the load acquired by the tensile machine and  $A(t)$  is the specimen cross sectional area instantaneous variation.

Finally, the Young's modulus was defined by dividing stress by strain as follows:

$$E = \sigma/\epsilon_l \text{ [MPa]} \quad (5.3)$$

It is the slope of the stress strain curve in the linear region.

Poisson ratio was defined as the transversal strain  $\epsilon_t$  divided by true longitudinal strain  $\epsilon_l$ :

$$\nu = - \epsilon_t/\epsilon_l \text{ [Adimensional]} \quad (5.4)$$

Transversal strain:

$$\epsilon_t = \ln[\text{width}(t)/\text{width}0] \quad (5.5)$$

Where  $\text{width}(t)$  is the instantaneous specimen width variation and  $\text{width}0$  is the initial specimen width.

These stress-strain curve was obtained as result for MCL and LCL (Figure 5.3) and the relative Young's modulus and Poisson ratio obtained are shown in the following table (Table 5.1).

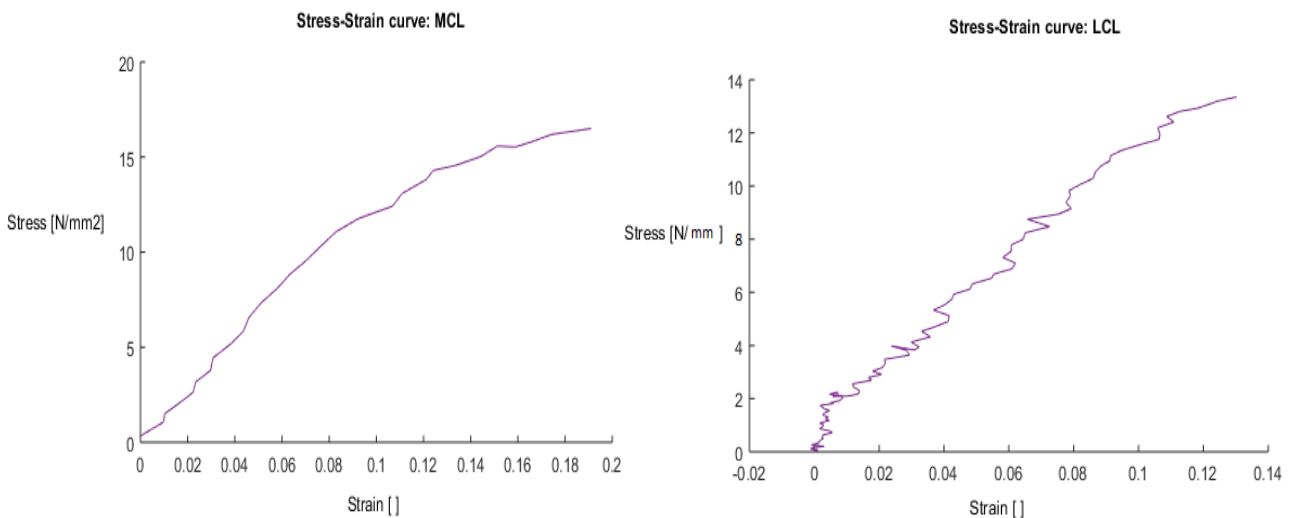


**Figure 5.3:** (left) MCL stress-strain curve; (right) LCL stress-strain curve. The results shown take in account the two middle (number 2 and 3).

Ligaments	Young's Modulus [MPa]	Poisson's Ratio
LCL	120	0.45
MCL	140	0.45

**Table 5.1:** Experimental results of the mechanical characterization of the medial and lateral collateral ligaments.

Comparing this outcomes with parameter found in the literature, it's clear that they have a high laxity. During the experimental test, in fact, the MCL was damaged by the saw used to implant the prosthesis and the LCL was already a lax ligament, not good for a TKA implant.

This fact demonstrates that a patient specific characterization of the soft tissues is necessary to reproduce a finite element model that allows to have outcomes as close as it's possible to the experimental findings.

# Chapter 6

## Numerical modelling

### 6.1 Introduction to the Finite Element Analysis

Finite Element Analysis (FEA) is a numerical procedure that can be used to obtain solution to a large class of engineering problems involving stress analysis, heat transfer, electromagnetism and fluid flow.

In general, mathematic problems are mathematical models of physical situations. Mathematical models are differential equations with a set of corresponding boundary and initial conditions. The differential equations are derived by applying the fundamental laws and principles of nature to a system or a control volume.

Unfortunately, there are a lot of engineering problems for which it is impossible to find the exact solution, due to the complexity of the differential equations or the difficulty in dealing with the boundary and initial conditions. For these problems it is necessary to use a numerical approximation as FEA.

The FEA is based on a discretization of space of the system to be analysed in sub-regions and nodes in which integral formulation is used to create a system of algebraic equations. Moreover, an approximate continuous function is assumed to represent the solution for each system element.

### 6.2 FEA in biomechanics

The field of orthopaedics biomechanics utilises two major numerical approaches: *musculoskeletal research* is based on multi-body-dynamics, dealing with kinematics of the skeletal system and muscle activity [41]. The second, *structure-mechanical point of view* deals with stress and strain analysis of bone, joint (natural and artificial) and load-bearing implant [42]. Finite Element Analysis is the preferred method for this second group of numerical problems occurring in orthopaedic biomechanics. Due to the resolution of the calculated mechanical parameters, the results get more accurate the more elements the analysed structure is divided into. To be useful in orthopaedic applications, the FEA results has to gain a clinical relevance for the clinician which is the subject the study is intended to. Naturally, despite very few exceptions, the FE analysis are engineers, who need to make their result understandable to a clinician not familiar with numerical simulation. The key for a fruitful communication between the clinician and the engineer is the reciprocal language, overall the principal terms, in order to allows the engineer to set correctly the FEA parameters and the clinician to know the potential and it falls of the FEA. By following these guidelines, a curriculum of the 'input' of relevant clinical questions and prevision of solutions with analytical background can be achieved.

Another important aspect of the FEA use for biomechanical applications is that the analysed structures are not man-made but of biological origin. There is not a standard or exactly defined shape of the structure, but it has a patient-specific morphology depending on many factors as age, physiologic loads, health and other many subjective attributes.

Bone morphology is mainly determined by genetic factors, but also by mechanics, as discovered by the German orthopaedic surgeon Julius Wolff (1892). Wolff's law states that bone has the ability to adapt to mechanical loads, i.e. the external and internal structure of bone is transformed depending on the load occurring in the bone [43]. Especially with regard to implant technology and arthroplasty, bone transformations play an important role. If the biomechanical distribution of forces in and around the treated joint is reconstructed inappropriately during surgery, or if the design of the implant is improper, so-called "stress-shielding" can occur. If the forces are mainly transferred by the implant, adjacent bony regions get minimally loaded and are remodelling itself and increasing its volume and density [44].

Because of these issues, FEA can find an important application to achieve the stress and strain on implant-bone compound [45].

## **6.3 Biomechanical FEA model generation**

The setup of FEA model consists in different steps that have to be followed in order to characterized from the "microscopic" properties (mechanical properties of the materials involved, the geometry structure) to the macroscopic once (the movement imposed to the assembly, constraints). The following sections will explain deeply each needed step to build up a FEA model.

### **6.3.1 Geometry**

The native knee model geometry is based on Computed Tomography (CT) and Magnetic Resonance Imaging (MRI) scans of one intact fresh-frozen left native knee cadaveric specimen.

In particular, to identify the femur and tibia bones, a helical CT scan is used (CT setting: 120kV, 210 mA, slice thickness of 0.6 mm, pitch of 0.6 mm/rev and a spiral pitch factor of 1) while, to identify the lateral collateral ligament (LCL) and the medial collateral ligament (MCL) an MRI is performed (MRI setting: TE: 39 ms, TR: 1300 ms, slice thickness: 0.5 mm, flip angle 160°, ETL: 139 and NP:154). The CT and MRI images are imported in an image processing software (ScanIP, Simpleware, Exeter, UK) to extract the geometry and to generate 3D models of all the structures following the steps below:

- a) segmentation of the cortical and cancellous bone from CT scans (Figure 6.1);
- b) filtering of the surface obtained for a smoother and more regular geometry. A Gaussian filter was used (Figure 6.2);
- c) generation of the surfaces;
- d) exportation of the IGES files (.iges).

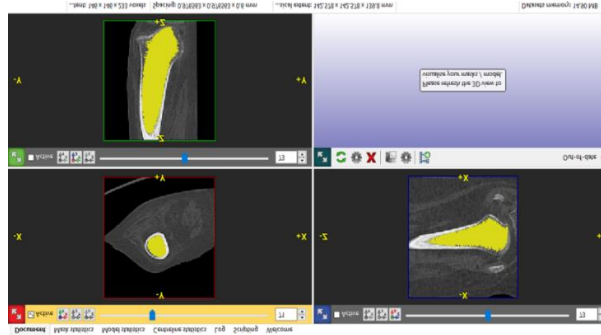


**Figure 6.1:** Segmentation of CT scans of the femur.

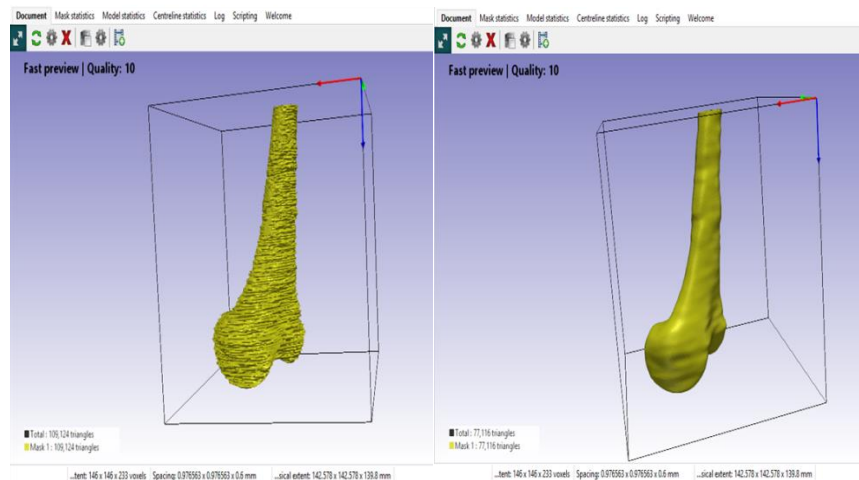


**Figure 6.2:** (left) Femur segmentation before smoothing filtering; (right) Femur segmentation after smoothing filtering.

With regard to the modeling of the ligaments, the MRI scans resolution was too low and the ligaments weren't visible as much as it could be possible the segmentation of the images. The geometry of ligaments was generated as Beam directly in the FE software Abaqus Standard Version 6.12-1 (Dassault systems, vélizy-Villacoublay, France).

The TKA geometry was obtained using the CAD file of the prosthesis. The CAD file was chosen according to the sizes needed for the specific knee joint. In this project were chosen:

- a) as femur component a 5 size;
- b) as tibial component a 4 size with 11 mm as insert.

The following landmarks were identified on the femur and tibia bones (Table 6. ). In particular the attachment and insertion sites for the LCL and MCL were identified using the the image processing software (ScanIP, Simpleware, Exeter, UK) according to the literature [46].

### 6.3.2 Positioning and orientation of the model

The landmarks coordinates in both experimental and numerical environment were useful to find the initial correct position of the FE implanted knee model.

All the landmarks coordinates were defined in CAD software Abaqus Standard Version 6.12-1 (Dassault systems, vélizy-Villacoublay, France). Translating and rotating the landmarks from the

numerical model and the model itself to the relative position in the experimental coordinates, the correct position was reached (Figure 6.3).

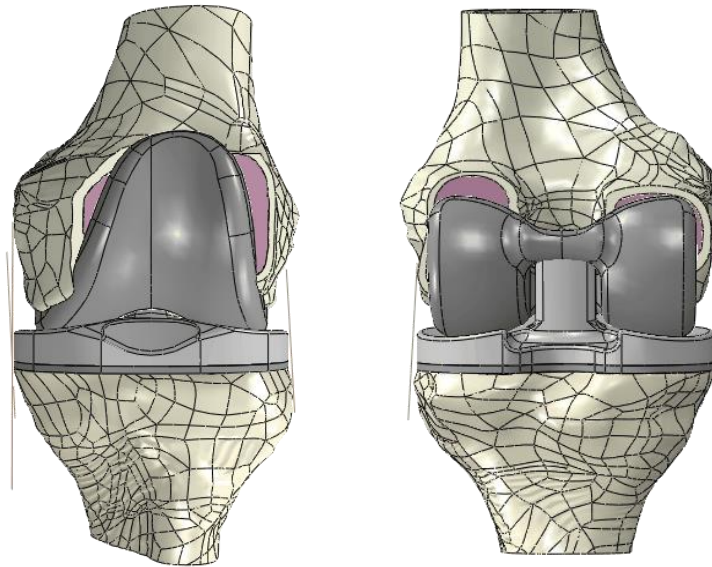


**Figure 6.3:** (left) Abaqus model from front point of view; (right) Abaqus model from back point of view.

### 6.3.3 Materials properties definition

A literature review, based on experimental and numerical papers, was conducted in order to collect information about the material behaviour of bones and ligaments. For these tissues, a linear elastic model resulted suitable to be applied for the simulated task. Unfortunately, the literature review, comprehensive of experimental and numerical papers, resulted in heterogeneous values to describe the material properties of every investigated tissue.

#### a) Knee bones

Bones support the body and cradle the soft organs, protect vital organs, allow movement, store minerals such as calcium and phosphate, and house hematopoietic tissue in specific marrow cavities. The fact that bone is a living material that could heal itself was documented over 5000 years ago from ancient Egyptians. From the past years, the mechanical and material properties of the bone have been extensively characterized. Bone has a dense outer layer consisting of cortical (compact) bone that appears smooth and solid while internal to cortical bone there is trabecular or spongy bone, which consists of honeycomb, needle-like, or flat pieces, called trabeculae (Figure 6.1).

The structural and the material properties of cortical and spongy bones are different due to the relative characteristic porosity of the two. Generally, the properties of the bone are not constant: strength, modulus, and density can vary between individuals, anatomic locations, and as result of age or disease process. In the literature, bone has been modelled similarly as rigid or linear isotropic material aiming for the development of computational knee models. It has also been suggested that the rigid bone assumption in knee joint models should create changes less than 2-3% in estimated contact pressure as compared to those assuming bone as an elastic deformable tissue. Moreover, literature reports that the nature of the elastic

properties assigned to the bones has only a marginal influence on final stress analysis. In order to develop subject-specific knee models for finite element analysis, different material mapping strategies have been followed in the years to automatically attribute material properties to bone models basing on CTs. Even if the assessment of bone mineral density and mechanical properties can be assessed with CT, unfortunately, the resolution of clinical CT equipment is often insufficient to resolve trabecular structure architecture, but still material properties such as Young Modulus can be estimated. It has also been observed that tibiofemoral contact parameters, stresses, strains, and pore pressures are highly independent on the implemented properties of trabecular bone. Considering the final outputs that will be analysed after a FEA of the subject specific knee model, the bone material has been considered homogeneously linearly deformable. Adopted material properties are shown in the following table (Table 6.1-2).

Cortical bone	Young's Modulus [MPa]			Poisson's Ratio			Shear Modulus [MPa]			Density [g/cm <sup>3</sup> ]
	E <sub>1</sub>	E <sub>2</sub>	E <sub>3</sub>	v <sub>12</sub>	v <sub>13</sub>	v <sub>23</sub>	G <sub>12</sub>	G <sub>13</sub>	G <sub>23</sub>	
Physiological	11500	11500	17000	0.51	0.31	0.31	3.8	4.4	4.4	1.8
Osteopenic	9660	9660	14280	0.51	0.31	0.31	3.2	3.7	3.7	1.6
Osteoporotic	7820	7820	11560	0.51	0.31	0.31	2.6	3	3	1.4

**Table 6.1:** Cortical bone mechanical properties estimation from literature [47].

Cancellous bone	Young's Modulus [MPa]	Poisson's Ratio	Density [g/cm <sup>3</sup> ]
Physiological	2130	0.3	0.13
Osteopenic	1427	0.3	0.10
Osteoporotic	724	0.3	0.8

**Table 6.2:** Cancellous bone mechanical properties from literature considering different bone condition [48]. Considering these specimens was modelled a physiologic bone.

#### b) Ligaments

In the literature is reported that ligaments cannot be characterized all with the same properties even if they can follow similar material behaviours. Yet, in order to be able to associate the right material properties, an in-depth literature research was necessary and was mainly directed to parameters already used for finite element analyses. Then, the literature search has been deepened to identify the original sources of the material properties. Linear elastic isotropic behaviour has been chosen for all the ligaments, but with different material properties as related to the literature research. For the collateral ligaments, the average elastic modulus has been evaluated as the mean between the moduli of the numerical studies. Poisson coefficient is considered positive and equal to 0.45 for all the ligaments, as reported by the majority of the literature studies [49,50].

The mechanical properties were compared and checked with the experimental values obtained from the Tensile Test. The following table resume all the literature and experimental findings (Table 6.3).

Ligaments	Literature			Experimental findings	
	Young's Modulus [MPa]	Poisson's Ratio	Density [g/cm <sup>3</sup> ]	Young's Modulus [MPa]	Poisson's Ratio
LCL	280	0.4	3.1	120	0.4
MCL	224	0.4	3.1	140	0.4

**Table 6.3:** Cancellous bone mechanical properties from literature compared with experimental outcomes, exception for the density.

Moreover, all the ligaments are modelled also in their pre-strain characteristic, considering the values reported in the literature [51]. The importance of considering the pre-strain is reported in literature to affect the outputs proving reliable stability during the simulated tasks. That behaviour was modelled as a temperature field that inducing a heat contraction makes the ligaments in tension at the beginning of the simulation.

#### c) Prosthesis

With regards to the materials properties of the implant, they are resumed in the following table (Table 6.4). The datasheet of the implant was taking in account in the mechanical properties definition.

TKA component	Literature		
	Young's Modulus [MPa]	Poisson's Ratio	Density [g/cm <sup>3</sup> ]
Femoral component (CoCr)	240.000	0.3	8.27166
Tibial polyethylene (PMMA)	724.2	0.2	9.2976
Tibial baseplate (CoCr)	240.000	0.3	8.27166

**Table 6.4:** Prosthesis mechanical properties.

### 6.3.4 Contact definition

To simulate the interaction between all the bones and the insert components a surface to surface contact was defined. For this reason different surfaces were identified with regard to the contact taken in account for the analysis. On these surfaces the contact area and contact force were extracted.

### 6.3.5 Boundary conditions

The simulation starts with the extended joint. To simulate the passive movement, there are no forces applied to quadriceps and hamstrings. For this reason the patella was excluded from the model. The ankle forces, measured as reaction forces during the experimental test from the Oxford rig, were simulated by external loads applied to the femur. The right direction and versus of the experimental ones was taking in account. The flexion-extension movement was applied according to the experimental outcomes. During the flexion-extension movements the Tibia bone was kept fixed (Figure 6.4).

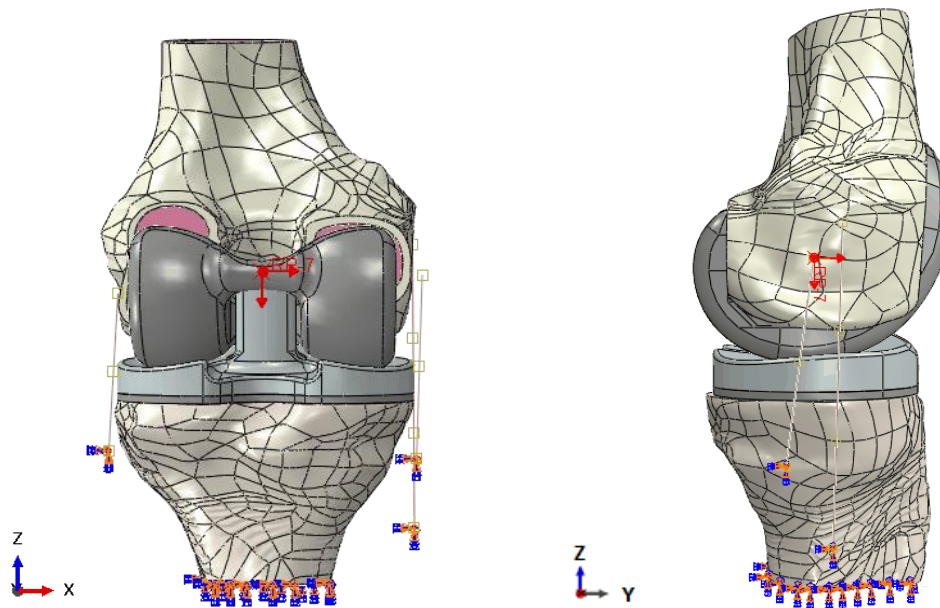


**Figure 6.4:** Loads and constraints in Abaqus.

### 6.3.6 Mesh of the model and outputs request

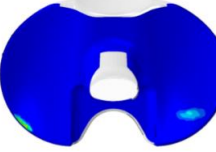
The mesh was defined using tetrahedral elements characterized by different elements size according to the region of interest. A quadratic order is chosen (Figure 6.5). A convergence test is performed to check the element size mesh quality. Abaqus Standard Version 6.12-1 (Dassault systems, vélizy-Villacoublay, France) is used to perform all the finite element simulations. For the defined model (the knee with TKA implant), the Von Mises stress in the proximal tibia, the load distribution between the medial and lateral compartments, the pressure and the contact area are extracted in tibio-femoral contact regions.



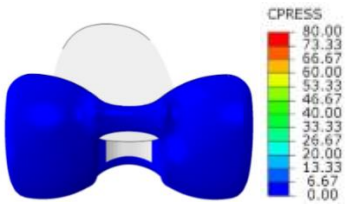
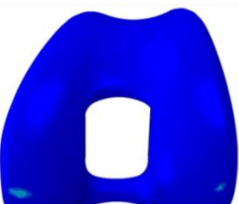
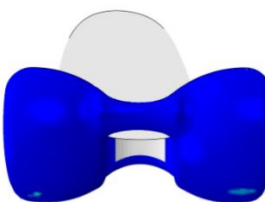
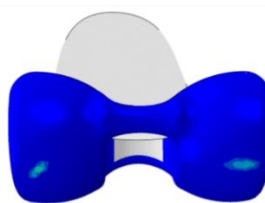
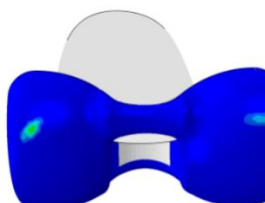
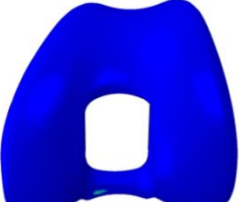
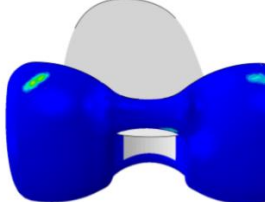
**Figure 6.5:** (left) Abaqus mesh model from front point of view; (right) Abaqus mesh model from back point of view.

### 6.3.7 Model parameters tuning

Previous results were obtained and compared to the experimental outcomes. They seemed to have a different behaviour and pressure higher than the expected. In fact, the average pressure obtained from the contact force divided by the contact area on the tibial insert reached value of about 20 MPa in the lateral plateau and 15 MPa in the medial plateau. In the experimental test the pressure stayed in the range of 6 MPa, with higher value in the medial plateau. The following tables (Table 6.5-6) shows the results in terms of contact pressure measured on the tibial insert and on femoral component, while the figure 6.6 reports the average contact pressure during the flexion-extension movement.

Tibial insert	Contact pressure
0°	
20°	
30°	
60°	
90°	
120°	

**Table 6.5:** Previous results in terms of contact pressure obtained on the tibial polyethylene insert. Left side is the lateral plateau; right side is the medial plateau.

Femoral component	0°	90°
0°		
20°		
30°		
60°		
90°		
120°		

**Table 6.6:** Previous results in terms of contact pressure obtained on the femoral component.

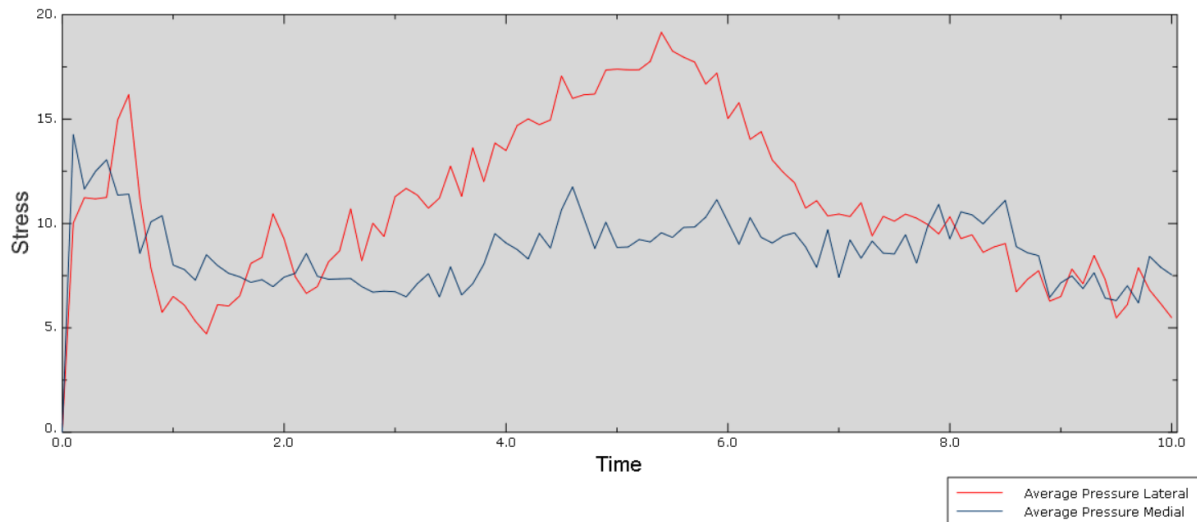


**Figure 6.6:** Average contact pressure during the flexion-extension movement on the lateral (red) and medial (blue) plateau.

Instead, in terms of kinematic, analysing internal-external rotation of the femur on the tibia, it is possible to observe 7° of external rotation during the knee flexion, while during the extension movement the femur shows 1° of internal rotation on the tibia at the end of the observed movement. Results performed on the numerical model of the same analysed specimen and for similar boundary conditions report a similar internal/external kinematics trend with a range of degrees of external rotation (Figure 6.7).

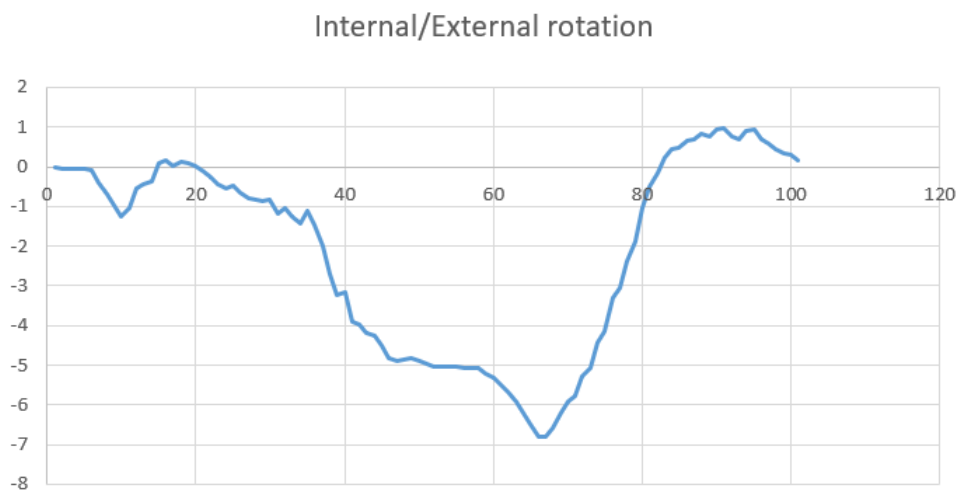


**Figure 6.7:** Internal/external rotation of femur with respect to the tibia.

A possible explanation of the differences previously reported could be the fact that the model was built using a prosthesis that wasn't the same of the experimental test. In the numerical model two sizes were modelled, 4 size for the tibial components and size 5 for the femoral component. The fact is that different implants can react in different way if coupled with components of different sizes, even some times isn't possible to coupled different sizes of a specific implant. Specifically, in this model a Link PS TKA was used. In the experimental test a Genesis by Smith and Nephew was used.

In this case the tuning of the model consisted on using the 5 size for each component, avoiding a concentration of the forces in small surfaces that can lead to contact pressure too high (Figure 6.8).

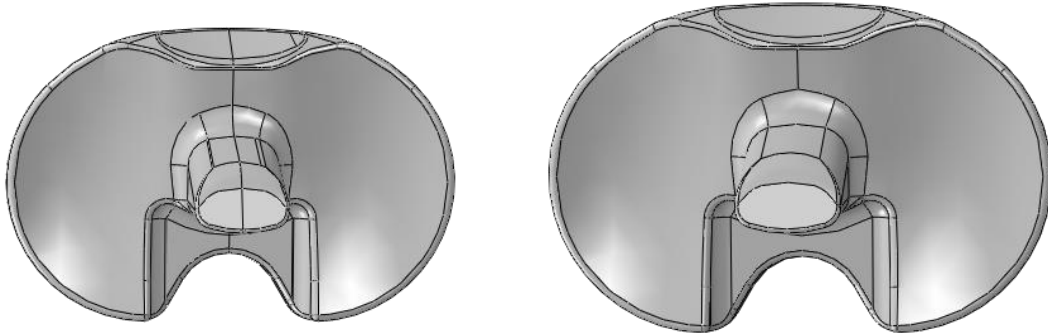


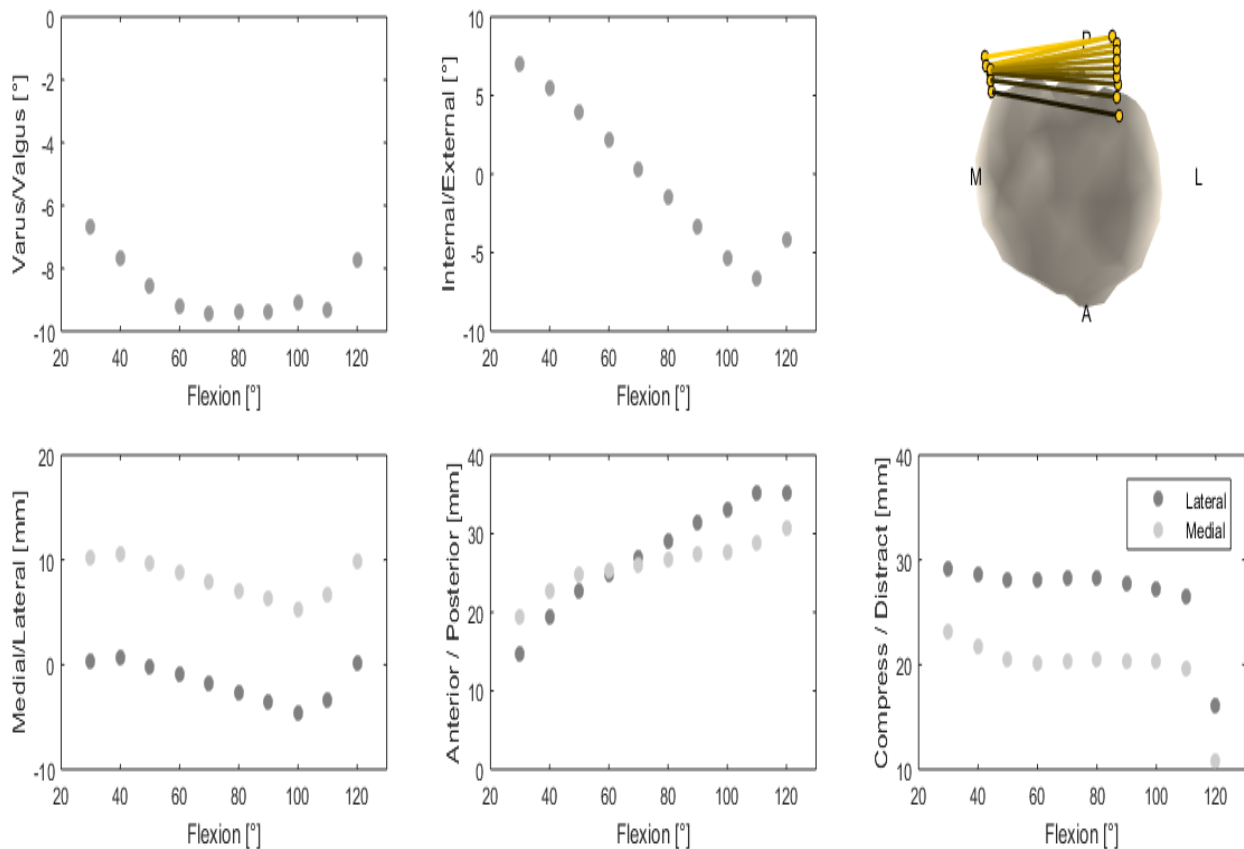
**Figure 6.8:** (Left) Tibial implant: size 4; (Right) Tibial implant: size 5.

# Chapter 7

## Outputs and comparison between Experimental and Numerical model. Validation of the test Protocol

### 7.1 Results

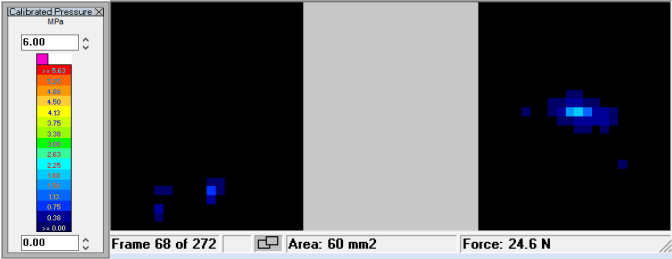
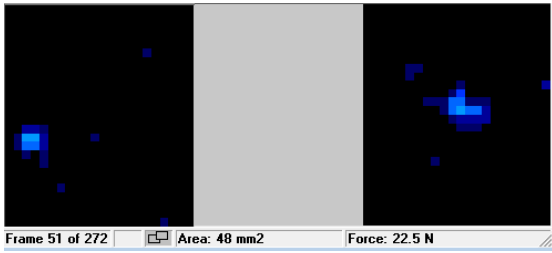
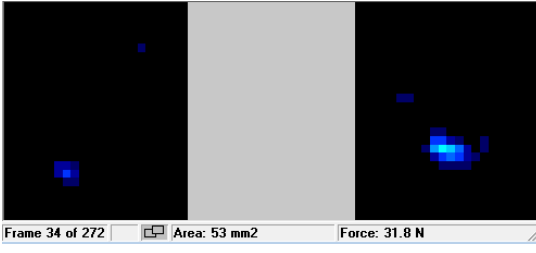
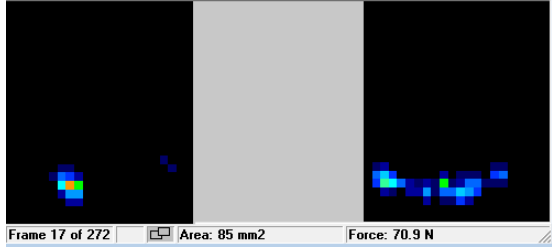
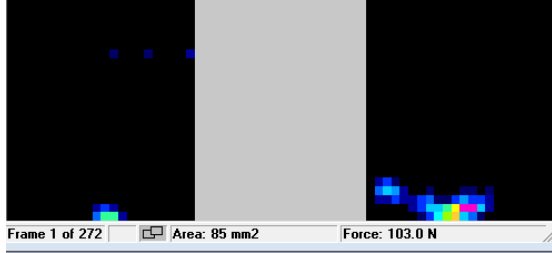
In passive conditions, from 20°-120° of flexion, the femur rotated externally with increasing flexion, to an average of 7.5°. Furthermore, during the flexion-extension movement the medial and lateral condyles gradually move laterally, totalling 4 mm of translation. Moreover, the femoral-tibial anterior-posterior translation is posteriorly oriented with increasing knee flexion in an average value of 10 mm for the medial condyle and 25 mm for the lateral condyle (Figure 7.1).



**Figure 7.1:** Translation (mm) and rotation (°) plots as a function of the flexion angle for the passive flexion-extension passive movement experimentally tested.

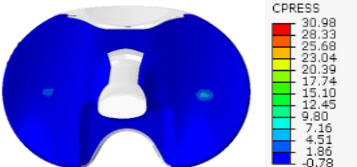
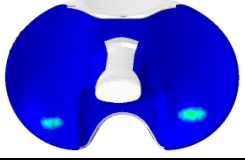
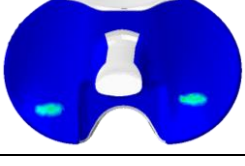
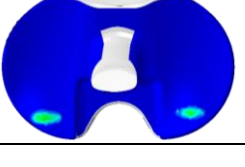
Furthermore, the contact pressures involved on the tibial insert measured with the Tekscan sensor are reported in the following table (Table 7.1). The pressure increases with flexion achieving values in a range between 0 to 10 MPa. Maximum values of pressures are mainly located on the medial side up to 60° of flexion; from 60° to 120° the lateral side undergoes a higher value of pressure than the first part of the movement. The contact zone moves from anterior to posterior especially

in the first 60° of flexion being later located in the posterior part for the rest of the flexion movement.

Flexion angle	Tekscan measurements
0°	
30°	
60°	
90°	
120°	

**Table 7.1:** Tekscan measurements of the tibio-femoral contact pressures, forces and area reported for different flexion angle during passive movements.

Moreover, results from numerical simulation performed on the model of the same analysed specimen and for similar boundary conditions are shown in table 7.2 in terms of contact pressure on the tibial insert for the observed range of movement. Contact pressure increases with flexion achieving values in a range between 0 and 15 MPa. Maximum values of pressure are mainly located on the medial side up to 60° of flexion; from 60° to 120° starts increasing also in the lateral side. Table 7.3 reports the contact pressure on the femoral component. The contact zone moves from anterior to posterior especially in the first 20° of flexion being later located in the posterior part for the rest of the flexion movement. Reported contact pressures are in a range of 0-20 MPa. The average pressure was obtained dividing the contact force measured in different region of interest with the specific contact area. The result about the average contact pressure are shown below (Figure 7.2). The result obtained are similar in terms of amplitude and behaviour to experimental findings.

Tibial insert	Contact pressure
0°	
20°	
30°	
60°	
90°	
120°	

**Table 7.1:** Contact pressure on tibial insert in different angle of flexion and from different point of view. Lateral side on the left; Medial side on the right.

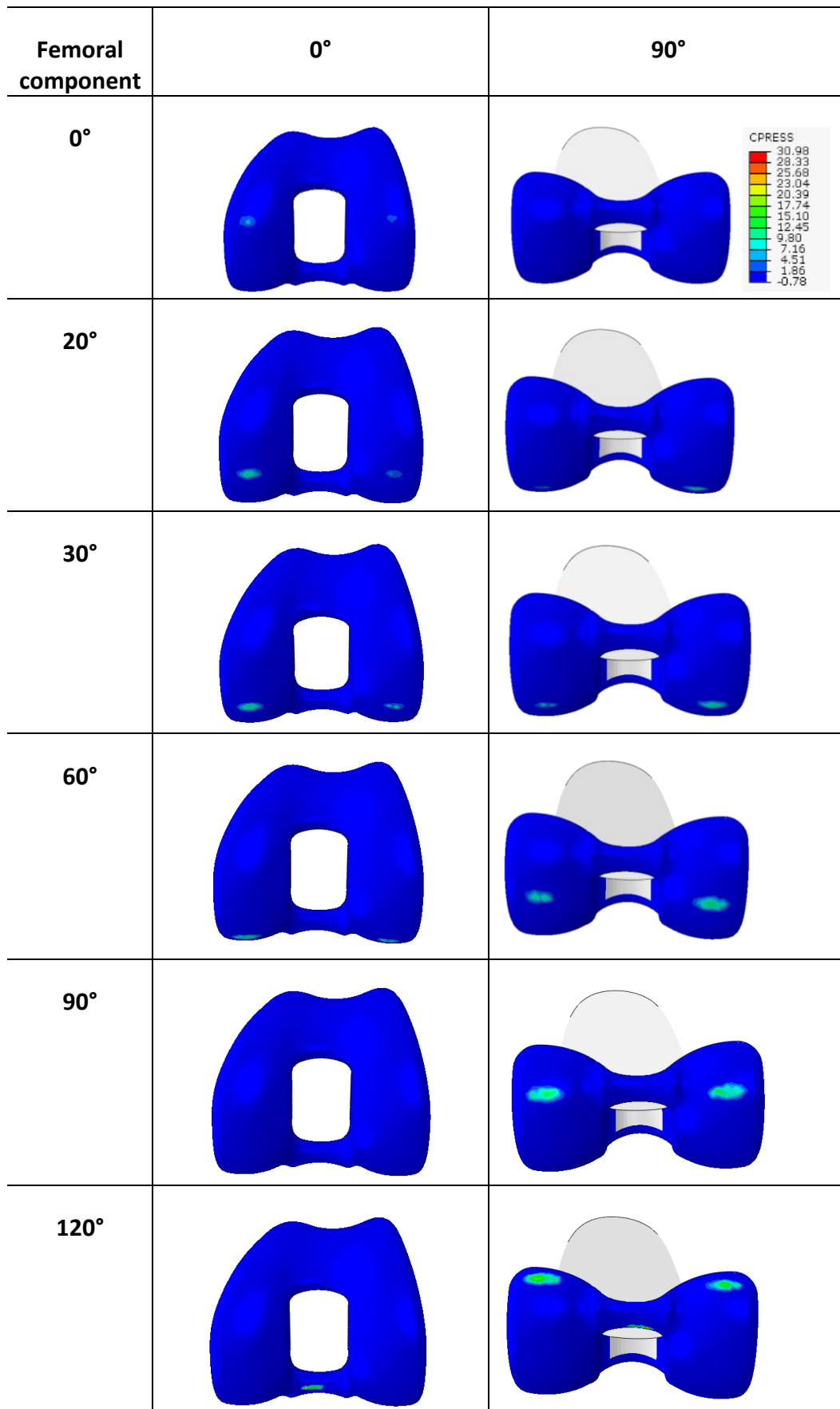


**Table 7.3:** Contact pressure on femoral component in different angle of flexion and from different point of view.

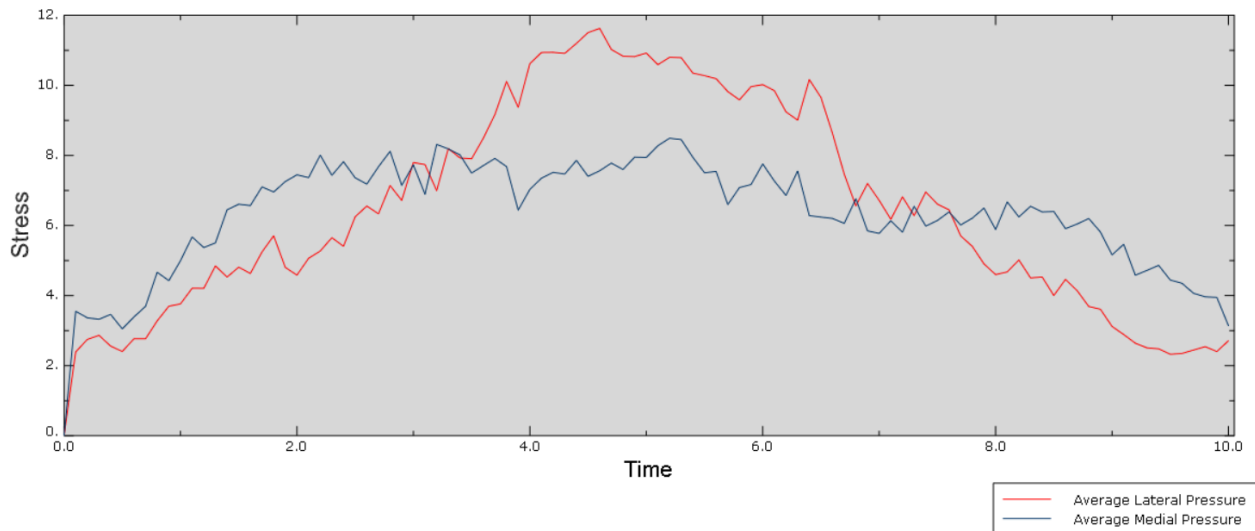


**Figure 7.2:** Average pressure measured on lateral (red) and medial (blue) plateaux during the flexion-extension movement on the tibial insert.

Furthermore, Femoral-tibial anterior-posterior translation is posteriorly oriented with increasing knee flexion in average range of 20 mm in agreement with values reported experimentally. The posterior translation is higher for the lateral side than the medial side. In complete flexion the values reached are 22 mm and 15 mm respectively (Figure 7.3). Medial-lateral translation is in a range of 1.5 mm.

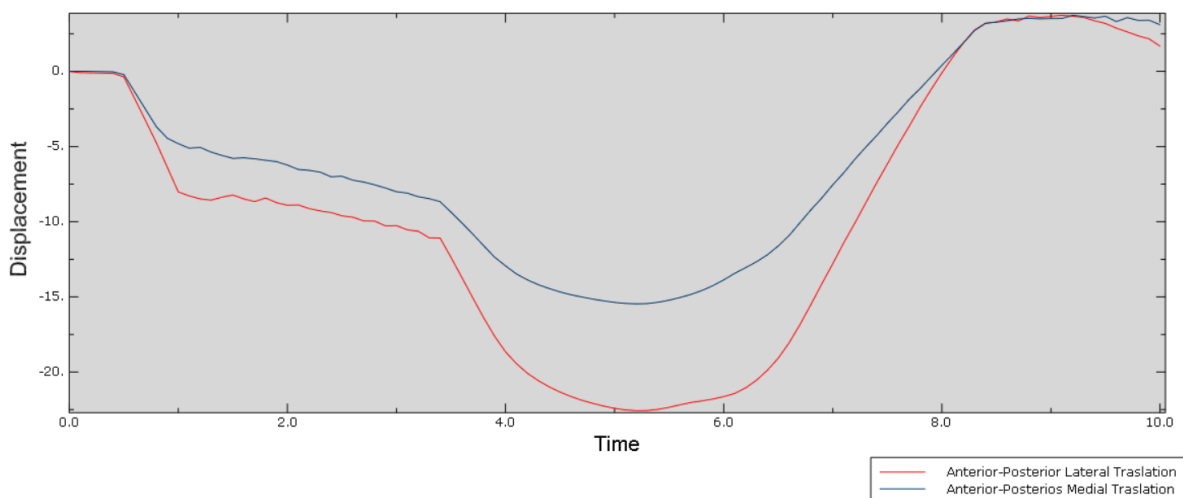


**Figure 7.3:** Anterior-posterior displacement (mm) plot as a function of the simulation period for the passive flexion-extension movement numerically obtained.

Analysing internal-external rotation of the femur on the tibia, it is possible to observe 3° of external rotation in the first 90 of knee flexion, while after the femur shows 4° of external rotation on the tibia up to the end of the observed movement. Also in this case the results shows similar behaviour.

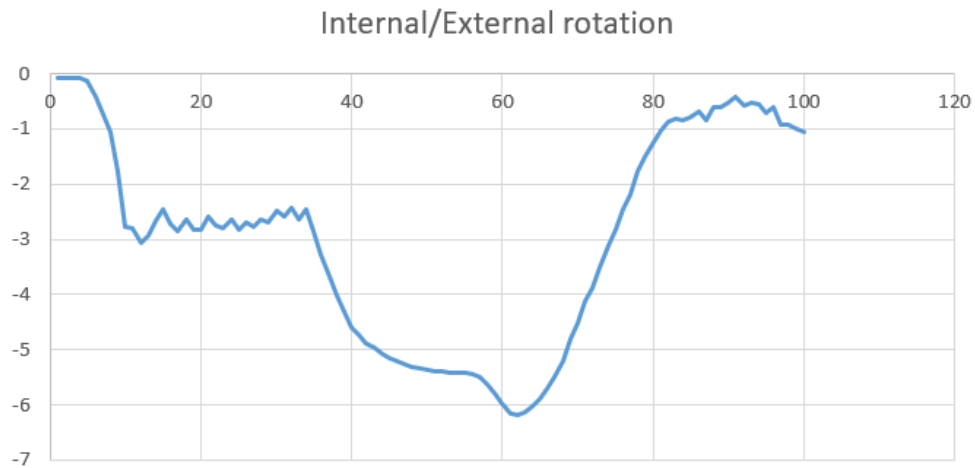


**Figure 7.3:** Internal/external rotation of femur with respect to the tibia

Under the comparison of the kinematical outputs obtained experimentally and numerically for the same reconstructed specimen under the same boundary conditions and considering also the agreements found with the showed contact pressure, the model could be considered reliable. With the validation of this numerical model, the experimental protocol for validate and verify a patient specific TKA FE model is also validated.

# Chapter 8

## Conclusion

In defining a patient specific model of an implanted knee, a definition of a complete protocol may represent a huge help in order to avoid particular difficulties that characterized the experimental tests. It may represent a useful guideline to obtain numerical models that are able to predict realistic behaviour of the knee joint in term of patient specific kinetic and kinematic [52]. This study proposes an experimental protocol verified and validated during a passive flexion-extension movement of an TKA implanted knee that provides step by step the procedure for doing the experimental test on the Oxford rig of the cadaver specimen, the tensile testing of the ligaments needed to obtain their mechanical properties and the reconstruction of the numerical patient specific model with the related material and boundary conditions definition. Results reported in this work show that, assuming similar boundary condition between the experimental test and the numerical simulation, personalized outputs can be obtained from a patient specific FE model following the protocol proposed in this analysis.

## Discussion and future development

Looking into clinical and research papers about the knee behaviour investigation, we are all aware that there is still missing information about the knee behaviour under several conditions. This lacking knowledge could be a possible explanation for failures and discontent for some patients after corrections of knee pathologies, such as when a TKA surgery is performed. As for other fields with respect to the biomechanical one, the use of numerical modelling is proved to provide fundamental support to simulate and predict situations that cannot be otherwise predicted, such as the stresses behaviour determination for the different structures of the joint under specific boundary conditions. Additionally, numerical simulations allow to perform a huge number of combinations for sensitivity analysis in a systematic way. Furthermore, the most challenging aspect is predicting subject-specific biomechanics or follow-up based on physiological conditions numerically modelled with unknown parameters. With the aim of analysing different knee biomechanical aspects, macro and micro numerical models are nowadays developed in almost parallel ways as the merging of their findings seems rarely practically possible because they are implemented following different approaches and computational costs. When a macro knee model development is necessary, different methodologies can be adopted, such as the rigid-body and the finite element analysis. Depending on the selected numerical approach, different approximations can be followed, but, up to now, there is no proof of how and how much the assumptions can influence the final outputs. Unfortunately, this is a critical point, because the results from numerical simulations are more and more often used to find possible explanations to unanswered clinical or industrial questions. The balance between the demand of subject-specific knee models and their accepted accuracy is delicate. However, defining the equilibrium is necessary considering several aspects such as inputs availability, material behaviour knowledge, boundary conditions replications, experimental data accuracy for comparison. For these reasons, the principal aims of this research have been to assess an experimental protocol in order to provide guidelines to identify an efficient way to reach result coherent with experimental findings.

## References

- [1] Silvia Pianigiani, Stéphane Godet, Loa Malet, Luc Labey, De Corte Ronny, Walter Pascale, Bernardo Innocenti, *Mechanical characterization of the soft tissues of a native human knee: a pilot study*, Journal of sports science, 2014, volume 2, pp 173-180.
- [2] Jan Victor, Francis Van Glabbe, Jos Vander Sloten, Johan Bellemans, *An experimental model for kinematic analysis of the knee*, Journal of bone and joint surgery-American volume, 2009, volume 91a, pp 150-163.
- [3] Silvia Pianigiani, Yan Chevalier, Luc Labey, Valerio Pascale, Bernardo Innocenti, *Tibio-femoral kinematics in different total knee arthroplasty designs during a loaded squat: A numerical sensitivity study*, Journal of biomechanics, 2012, Volume 45, 2315-2323.
- [4] Silvia Pianigiani, Yan Chevalier, Luc Labey, Walter Pascale, Bernardo Innocenti, *Effects of component malpositioning and soft-tissue balancing in Total Knee Arthroplasty kinematics*, Knee surgery sports traumatology arthroscopy, 2012, volume 20, pp 1183-1217.
- [5] Bernardo Innocenti, Evelyn Truyens, Luc Labey, Pius Wong, Jan Victor, Johan Bellemans, *Can medio-lateral baseplate position and load sharing induce asymptomatic local bone resorption of the proximal tibia? A finite element study*, Journal of orthopaedic surgery and research, 2009, pp 4-26.
- [6] Silvia Pianigiani, Luc Labey, Walter Pascale, Bernardo Innocenti, *Knee kinetics and kinematics: what are the effects of TKA malconfigurations?*, Knee surgery sports traumatology arthroscopy, 2016, volume 24, pp 2415-2421.
- [7] Bernardo Innocenti, Silvia Pianigiani, Gaetano Ramundo, Emmanuel Thiempont, *Biomechanical effects of different varus and valgus alignment in medial unicompartimental knee arthroplasty*, The Journal of arthroplasty, 2016, volume 31, pp2685-2691.
- [8] E.S. Grood, W. J. Suntay, *A joint coordinate system for the clinical description of three-dimensional motions: application to the knee*, Journal of biomechanical engineering, 1983, Volume 105, pp 136-144.
- [9] Brian A. Knarr, Jill S. Higginson, Joseph A. Zeni, *Change in knee contact force with simulated change in body weight*, Computer methods in biomechanics and biomedical engineering, 2016, volume 19, pp 320-323.
- [10] Mike D. Van Manen, James Nace, Michael A. Mont, *Management of primary knee osteoarthritis and indications for total knee arthroplasty for general practitioners*, The journal of the American osteopathic association, 2012, volume 112, pp 709-715.
- [11] Joshua Twiggs, Willy Theodore, Andrew Ruys, Justin Roe, David Dickinson, Brett Fritsch, Brad Miles, *Patient specific simulated dynamics following TKA correlate with patient reported outcomes*, EPiC series in health sciences, 2017, volume 1, pp 205-213.
- [12] Silvia Pianigiani, Lennart Scheys, Luc Labey, Walter Pascale, Bernardo Innocenti, *Biomechanical analysis of the post-cam mechanism in TKA: comparison between conventional and semi-constrained insert design*, International biomechanics, 2015, volume 2, pp 22-28.
- [13] Bernardo Innocenti, Yague Robledo H, Barbabe Alario R, Silvia Pianigiani, *Investigation on the effects induced by TKA features on tibio-femoral mechanics. Part I: femoral component design*, Journal of mechanics in medicine and biology, 2015, volume 15.

- [14] Bernardo Innocenti, Yague Robledo H, Barbabe Alario R, Silvia Pianigiani, *Investigation on the effects induced by TKA features on tibio-femoral mechanics. Part II: tibial component design*, Journal of mechanics in medicine and biology, 2015, volume 15.
- [15] Bernarndo Innocenti, Luc Labey, Amir Kamali, Walter Pascale, Silvia Pianigiani, *Development and validation of a wear model to predict polyethylene wear in a total knee arthroplasty: a finite element analysis*, Lubricans, 2014, volume 2, pp 193-205.
- [16] Jean Brihault, Alessandro Navacchia, Silvia Pianigiani, Luc Labey, Ronny De Corte, Valerio Pascale, Bernardo Innocenti, *All-polyethylene tibial components generate higher stress and micromotions than metal-backed tibial components in total knee arthroplasty*, Knee surgery sports traumatology arthroscopy, 2015, volume 24, pp 2550-2559.
- [17] Andrew L. Rosen, Giles R. Scuderi, *Patella resurfacing*, Techniques in knee surgery, 2002, volume 1, pp 72-76.
- [18] Brian K. Park, Wayne G. Paprosky, *Patellar resurfacing in total knee arthroplasty*, Seminars in arthroplasty, 2015, volume 26, pp 232-235.
- [19] Jonathan Noble, *Should the patella be resurfaced at total knee replacement?*, The knee, 2000, Volume 7, pp 199-204.
- [20] Shi-chang Chen, Yi-ming Zeng, Meng-ning Yan, Bing Yue, Jun Zhang, You Wang, *Effect of femoral component flexion implantation on the mediolateral bone-prosthetic fit in total knee arthroplasty*, Orthopedic surgery, 2017, Volume 9, pp 91-96.
- [21] Andrea Baldini, Pier Francesco Indelli, Lapo De Luca, Pierpaolo Cerulli Mariani, Massimiliano Marcucci, *Rotational alignment of the tibial component in total knee arthroplasty: the anterior tibial cortex is a reliable landmark*, Joints, 2014, volume 4, pp 155-160.
- [22] Jan Victor, Daisy Van Dominik, Luc Labey, Bernardo Innocenti, Johan Bellemans, *How precise can bony landmarks be determined on a CT scan of the knee*, The Knee, 2009, volume 16, pp 358-365.
- [23] Fabio Orozco, Alvin Ong, *Posterior stabilized total knee arthroplasty*, Recent advances in hip and knee arthroplasty, 2012.
- [24] Marco Schiraldi, Giancarlo Bonzanini, Danilo Chirillo, Vito de Tullio, *Mechanical and kinematic alignment in total knee arthroplasty*, Annals of translational medicine, 2016, volume 4.
- [25] Giles R. Scuderi, W. Norman Scott, Gregory H. Tchejyan, *The Insall legacy in total knee arthroplasty*, Clinical orthopaedics and related research, 2001, volume 392, pp 3-14.
- [26] Adrien Durandet, Pierre-Louis Ricci, Amir Hossein Saveh, Qureish Vanat, Bin Wang, Ibrahim Esat, Mahmoud Chizari, *Radiographic analysis of lower limb axial alignments*, Proceeding of the world congress on engineering, 2013, volume 2.
- [27] <http://www.smith-nephew.com/professional/microsites/navio/total-knee-arthroplasty/navio-total-knee/>.
- [28] W. Sampers, T. sierens, *Kinematic of the knee joint*, Sustainable construction and design, 2011.
- [29] Nele Arnout, Luc Vanlommel, Johan Bellemans, *Post-cam mechanics and tibio-femoral kinematics: a dynamic in vitro analysis of eight posterios-stabilized total knee designs*, Knee surgery sports traumatology arthroscopy, 2014, volume 22.
- [30] Claudio Belvedere, Alberto Leardini, Fabio Catani, Silvia Pianigiani, Bernardo Innocenti, *In vivo kinematics of the knee replacement during daily living activities: condylar and post-cam contact assessment by three dimensional fluoroscopy and finite element analyses*, Journal of orthopaedic research, 2016, volume 35.
- [31] A viscoelastic poromechanical model of the knee joint in large compression,.

- [32] M. Kazemi, L. P. Li, Bernardo Innocenti, Omer Faruk Bilgen, Luc Labey, Fabio Catani, *Load sharing and ligament strains in balanced, overstuffed and understuffed UKA. A validated finite element analysis*, The journal of arthroplasty, 2014, volume 29.
- [33] Silvia Pianigiani, Yan Chevalier, Luc Labey, Walter Pascale, Bernardo Innocenti, *Effects of component malpositioning and soft-tissue balancing in Total Knee Arthroplasty kinematics*, Knee surgery sports traumatology arthroscopy, 2012, volume 20, pp 1183-1217.
- [34] Silvia Pianigiani, Luc Labey, Walter Pascale, Bernardo Innocenti, *Knee kinetics and kinematics: what are the effects of TKA malconfigurations?*, Knee surgery sports traumatology arthroscopy, 2016, volume 24, pp 2415-2421.
- [35] Jan Victor, *A comparative study on the biomechanics of the native human knee joint and total knee arthroplasty*, Doctoral thesis in medical sciences, 2009.
- [36] Jan Victor, Daisy Van Dominik, Luc Labey, Bernardo Innocenti, Johan Bellemans, *How precise can bony landmarks be determined on a CT scan of the knee*, The Knee, 2009, volume 16, pp 358-365.
- [37] Matthias A. Verstraete, Laurent Willemont, Stefaan Van Onsem, Cyrielle Stevens, *3D printed guides for controlled alignment in biomechanics tests*, Journal of biomechanics, 2016, volume 49, pp 484-487.
- [38] Tony Chen, Hongsheng Wang, Bernardo Innocenti, *Tekscan measurements of interfacial contact area and stress in articulating joints*, Experimental methods in orthopaedic biomechanics, 2017, chapter 17, pp 267-283.
- [39] E.S. Grood, W. J. Suntay, *A joint coordinate system for the clinical description of three-dimensional motions: application to the knee*, Journal of biomechanical engineering, 1983, Volume 105, pp 136-144.
- [40] Bernardo Innocenti, Pierre Lambert, Jean-Charles Larrieu, Silvia Pianigiani, Marina Paolanti, Michele Bernardini, Annalisa Cenci, Emanuele Frontoni, *Development of an automatic procedure to mechanically characterize soft tissue materials*, Mechatronic and embedded systems and applications, 2016.
- [41] Yanhong Bei, Benjamin J. Fregly, *Multibody dynamic simulation of knee contact mechanics*, Medical engineering & physics, 2004, volume 26, pp 777-789.
- [42] M. Kazemi, L. P. Li, Bernardo Innocenti, Omer Faruk Bilgen, Luc Labey, Fabio Catani, *Load sharing and ligament strains in balanced, overstuffed and understuffed UKA. A validated finite element analysis*, The journal of arthroplasty, 2014, volume 29.
- [43] Julius Wolff, *The law of bone remodelling*, 1892.
- [44] Harry Van Lenthe, M C De Waal Malefijt, R Huiskes, *Stress shielding after total knee replacement may cause bone resorption in the distal femur*, The bone and joint journal, 1997, volume 79, pp 117-122.
- [45] Jean-Baptiste Renault, Sebatien Paratte, Patrick Chanbrand, *Stress shielding post total knee replacement, the influence of muscles. A finite element study*.
- [46] Bernardo Innocenti, Paolo Salandra, Walter Pascale, Silvia Pianigiani, *How accurate and reproducible are the identification of cruciate and collateral ligament insertions using MRI*, The Knee, 2016, volume 23, pp 575-581.
- [47] Jean Brihault, Alessandro Navacchia, Silvia Pianigiani, Luc Labey, Ronny De Corte, Valerio Pascale, Bernardo Innocenti, *All-polyethylene tibial components generate higher stress and micromotions than metal-backed tibial components in total knee arthroplasty*, Knee Surgery Sports Traumatology Arthroscopy, 2016, volume 24, pp 2550-2559.
- [48] Jean Brihault, Alessandro Navacchia, Silvia Pianigiani, Luc Labey, Ronny De Corte, Valerio Pascale, Bernardo Innocenti, *All-polyethylene tibial components generate higher*

- stress and micromotions than metal-backed tibial components in total knee arthroplasty, Knee Surgery Sports Traumatology Arthroscopy, 2016, volume 24, pp 2550-2559.*
- [49] M. Kazemi, L. P. Li, Bernardo Innocenti, Omer Faruk Bilgen, Luc Labey, Fabio Catani, *Load sharing and ligament strains in balanced, overstuffed and understuffed UKA. A validated finite element analysis, The journal of arthroplasty, 2014, volume 29.*
- [50] K.S. Halonen, M.E. Mononen, J. Töyräs, H. Kröger, A. Joukainen, R.K. Korhonen, *Optimal graft stiffness and pre-strain restore normal joint motion and cartilage responses in ACL reconstructed knee, Journal of Biomechanics, 2016, volume, pp 2566-2576.*
- [51] K.S. Halonen, M.E. Mononen, J. Töyräs, H. Kröger, A. Joukainen, R.K. Korhonen, *Optimal graft stiffness and pre-strain restore normal joint motion and cartilage responses in ACL reconstructed knee, Journal of Biomechanics, 2016, volume, pp 2566-2576.*
- [52] Bernardo Innocenti, *Knee biomechanics analysis and 3D modelling: to close the gap between surgeons and engineers.*

# Aknowloedgment

Questa tesi è il frutto di un lungo percorso personale. Sono state tante le fatiche e le difficoltà per rispondere alla faticosa domanda "chi voglio essere da grande?". E oggi spero, e dico così siccome un minimo di incertezza sarà sempre parte di me, è impossibile insomma bagnarsi due volte nello stesso fiume diceva qualche annetto fa un filosofetto da quattro soldi, di essere diventata una persona conscia del proprio valore, professionale sì, ma il valore umano è quello che mi interessa di più. Tutto questo lavoro per capire chi voglio essere però non è stato fatto solo da me. C'è chi mi ha illuminato la strada in questo mega tunnel pieno di buche. Mi hanno sostenuto nell'errore, nelle bocciature sempre prese in modo esageratamente personale e negativo, e hanno gioito più di me nelle mie vittorie.

Le persone che mi hanno accompagnato sono davvero tante e non riuscirei a citarle tutte dando il giusto merito ad ognuna, ma se stai leggendo questa pagina, sei stata una persona sicuramente che mi ha fatto crescere e mi ha regalato una parte di sé. Fai anche tu parte dei protagonisti di questo capitolo della mia vita. Forse il più importante.

Non posso però non citare Alberto ed Andrea. Nella mia vita di tutti i giorni, fin da quando eravamo piccoli, mi avete protetta e guidata. Mi avete fatto capire dove sbagliavo, sia come sorella che come persona, spingendomi a diventare giorno per giorno migliore.

Emiliano, ti cito solo perché mi ha citato nei tuoi ringraziamenti. Scherzo. Voglio solo dirti che è bello citarsi nello stesso tempo. Siamo cresciuti tanto e la mia stima verso di te non è mai mancata. Però inizia a lavare i pavimenti.

Non posso neanche non citare mamma e papà. Senza di voi tutto ciò non sarebbe stato possibile. Essere qui oggi tutti insieme, chi in un continente chi nell'altro, è importante, soprattutto perché poteva non essere così. Ed è questa una nostra grande vittoria. Quella più importante.

Con queste parole chiudo questa tesi, capitolo o esperienza a dir si voglia. Spero di avervi tutti sempre accanto, chi più vicino, chi più lontano. Con voi non solo ho costruito quella che sono oggi, ma sono sempre e comunque stata me stessa.